On singularities in non-Abelian black holes

D. V. Gal'tsov[a)]
M. V. Lomonosov Moscow State University, 119899 Moscow, Russia

E. E. Donets
Joint Institute of Nuclear Research, 141980 Dubna, Moscow Region, Russia

M. Yu. Zotov
Scientific Research Institute of Nuclear Physics, M. V. Lomonosov Moscow State University, 119899 Moscow, Russia

(Submitted 30 April 1997)
Pis'ma Zh. Éksp. Teor. Fiz. **65**, No. 12, 855–860 (25 June 1997)

Singularities in spherically symmetric black holes in the Einstein–Yang–Mills and the Einstein–Yang–Mills with dilaton theories for the $SU(2)$ group are investigated. Analytical formulas describing the exponentially oscillating and power-law behavior of the metric near a space-like singularity in a solution of the general form are presented. © *1997 American Institute of Physics.*
[S0021-3640(97)00112-6]

PACS numbers: 04.70.Dy, 04.20.Dw

Black holes in theories that include massless non-Abelian vector fields[1] exhibit properties which are unusual compared with ''classical'' vacuum and electrovacuum black holes. Besides violating the no-hair and uniqueness theorems, they exhibit a substantially new type of internal structure.[2] In Ref. 3 it was shown that the space–time inside a static black hole of general form in the $SU(2)$ Einstein–Yang–Mills theory (EYM) has no Cauchy horizons, and the metric oscillates with an amplitude that grows infinitely as the singularity is approached. Although some special solutions can still have a Schwarzschild or Reissner–Nordström (RN) type singularity,[3] these configurations form only a set of measure zero in the space of all solutions. Inside an EYM black hole of general form the mass function goes through a sequence of exponential jumps and drops. The amplitude of the peaks grows exponentially as the singularity is approached, while the period of the cycles approaches zero. The behavior of the system near a singularity is described well by a two-dimensional dynamical system,[3] from which the infinite oscillatory character of the solution is evident. These results were confirmed in Ref. 4, and a proof of the existence of RN-type solutions was claimed in Ref. 5. Our objective in the present letter is to clarify the structure of the singularity inside static spherical black holes of general form in the EYM and EYM with dilaton (EYMD) theories (see Ref. 6 and the references cited therein).

We choose the ''string'' value of the dilaton coupling constant and, with no loss of generality, fix the unit of measurement and scale of distances at which the Planck constant and the gauge coupling constant equal 1:

$$S=\frac{1}{16\pi}\int\{-R+2(\nabla\phi)^2-e^{-2\phi}F^2\}\sqrt{-g}d^4x, \tag{1}$$

where F is the $SU(2)$ field corresponding to the connection

$$A^a_\mu T_a dx^\mu=(W(r)-1)(T_\phi d\theta-T_\theta \sin\theta d\phi),$$

and T_ϕ and T_θ are the spherical projections of the $SU(2)$ generators.

It is convenient to represent the space–time interval in the form

$$ds^2=\frac{\Delta\sigma^2}{r^2}dt^2-\frac{r^2}{\Delta}dr^2-r^2(d\theta^2+\sin^2\theta d\phi^2), \tag{2}$$

where the function $\Delta=r^2-2rm(r)$ is negative inside a black hole of general form.

The equations of motion for W, Δ, and ϕ separate from the equation for σ, and in the general case of the EYMD system they can be represented in the form

$$\Delta U'-2\Delta U\phi'=WV/r-\mathcal{F}W', \tag{3}$$

$$(\Delta/r)'+\Delta\phi'^2=\mathcal{F}-2\Delta U^2e^{-2\phi} \tag{4}$$

$$(\Delta\phi')'+\Delta r\phi'^3=\mathcal{F}-2\Delta(\phi' r+1)U^2e^{-2\phi}-1, \tag{5}$$

where

$$U=\frac{W'}{r},\quad \mathcal{F}=1-\frac{V^2e^{-2\phi}}{r^2},\quad V=W^2-1.$$

The remaining equation for σ has the form

$$(\ln\sigma)'=r(\phi'^2+2U^2e^{-2\phi}). \tag{6}$$

Solutions of the black-hole type are engendered by initial data on the event horizon r_h, $W_h=W(r_h)$, and $\phi_h=\phi(r_h)$ which satisfy the condition $\mathcal{F}_h>0$. They can be characterized by the values of the Arnowitt–Deser–Misner mass M and the dilaton charge $D=-\lim(r^2\phi')$ as $r\to\infty$. It is convenient to fix the units of measurement for these quantities by requiring that $\phi(\infty)=0$. Then the asymptotic-flatness condition has the effect that both quantities W_h and ϕ_h assume a discrete series of values. For physical solutions of the black-hole type $M>D$.

Let us first study the structure of the singularity of the interior space of the exponentially oscillating type for black holes of general form in the EYM theory. In this case the system of equations assumes the form

$$\Delta U'+\left(1-\frac{V^2}{r^2}\right)W'=\frac{WV}{r}, \tag{7}$$

$$\left(\frac{\Delta}{r}\right)'+2\Delta U^2=1-\frac{V^2}{r^2}, \tag{8}$$

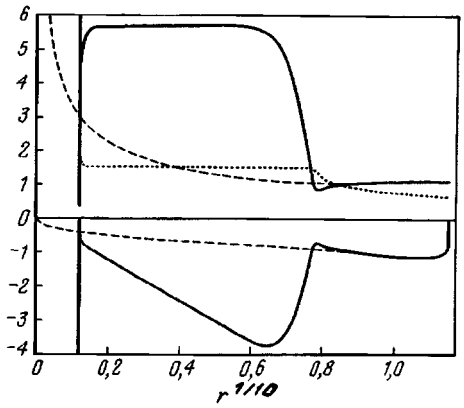

FIG. 1. Region of the first oscillation for EYM. Bottom half plane: the function Δ for EYM (solid line) and EYMD (dashed line); top half plane: the mass functions $m(r)$ (similarly) and the function U for EYM (dotted line). The values of all functions are raised to the power 1/10. $r_h=4$; $W_h=-0.283993$ for the EYM system, $W_h=-0.298357$, $\phi_h=0.05623$ for EYMD (asymptotically flat solutions with one zero of the function W in the exterior region).

$$\frac{d}{dr^2}\ln\,\sigma=U^2. \tag{9}$$

When this system is integrated numerically from the event horizon in the direction of decreasing radial coordinate, in the general case (with the exception of some discrete values of the initial data on the event horizon), the function Δ starts to oscillate. Once the oscillations have developed, the right-hand side of Eq. (7) becomes negligibly small compared with the terms on the left-hand side and the following approximate first integral of the system can be obtained:

$$Z=\Delta U\sigma/r=\text{const}, \tag{10}$$

which relates the oscillations of the mass function and the function σ. Numerical experiments also show that while the YM function W exhibits very small variations right down to $r=0$, its derivative is still different from zero and changes very rapidly in some very small intervals of r. The function U exhibits close to step-like behavior: It is constant, to a high degree of accuracy, during almost the entire oscillation cycle chosen (Fig. 1) and then changes abruptly to a higher absolute value corresponding to the next cycle. It is obvious from Eq. (9) that σ falls off exponentially with decreasing r, as long as $U\approx$const, while σ hardly changes on very small intervals during the jumps in U. Therefore σ approaches zero through an infinite sequence of exponential drops with increasing exponents on intervals of exponentially decreasing length. In combination with Eq. (10) and the above-indicated properties of U, this makes it possible to obtain a quite detailed description of the behavior of the metric.

We denote by r_k the value of the radial coordinate for which Δ reaches the kth local maximum. Soon after this point is crossed, the function U stabilizes at some value U_k,

approximately equal to twice the value at the point of the maximum (similarly, as a local maximum is approached, U approximately doubles while Δ is almost stationary). Then, in accordance with Eq. (9), σ equals

$$\sigma(r)=\sigma(r_k)\exp[U_k^2(r^2-r_k^2)].$$

From Eq. (10) we find that as long as $U_k\approx$ const

$$\Delta(r)=\frac{\Delta(r_k)}{r_k}r\ \exp[U_k^2(r_k^2-r^2)]. \tag{11}$$

This function decreases with r to a local minimum at the point

$$R_k=\frac{1}{\sqrt{2}|U_k|}\approx\frac{\sqrt{|\Delta(r_k)|}}{2|V(r_k)|}r_k. \tag{12}$$

Further, since the YM function W changes very little during the oscillations of the function Δ, we shall assume that $V=$ const.

Therefore, at the stage of exponential growth of $|\Delta|$the mass function grows exponentially as r decreases from r_k to R_k. After the point R_k is crossed, the exponential in Eq. (11) becomes close to 1 in order of magnitude, and therefore Δ starts to grow linearly and the mass function $m(r)$ remains at the value $M_k=m(R_k)$. This behavior remains up to the moment Δ/r^2 reaches its local maximum, which occurs for $\Delta\approx-V^2$ at the point

$$r_k^*\approx\frac{V^2}{|\Delta(r_k)|}r_k\ \exp[-(U_kr_k)^2]. \tag{13}$$

Then $|\Delta|$ drops rapidly, giving rise to rapid growth of $|U|$. The term $2\Delta U^2$ in Eq. (8) becomes negligibly small, as a result of which at this stage

$$U\Delta\approx-V^2U_k, \tag{14}$$

the coordinate r changing very little. This has the effect that the function Δ rapidly reaches the next local maximum at the point $r_{k+1}\approx r_k^*$ and $m(r)$ drops rapidly to m_{k+1}. In Eq. (8) $|\Delta|\ll V^2$ at the point of a local maximum of Δ, and since r is small, we find

$$|U(r_k)|\approx\frac{|V|}{\sqrt{2|\Delta(r_k)|}r_k}. \tag{15}$$

To obtain order of magnitude estimates we shall neglect the numerical coefficients everywhere except in the exponents of the exponentials. Specifically, we set $U(r_k)=U_k$ and drop the (quasiconstant) factors V. To this accuracy, we obtain from Eqs. (11)–(15)

$$r_{k+1}=M_k^{-1},\quad r_{k+1}^2=R_kR_{k+1},\quad M_k=\frac{R_k^2}{r_k^3}\ \exp\left(\frac{r_k^2}{2R_k^2}\right),$$

$$|\Delta(r_k)|=\left(\frac{R_k}{r_k}\right)^2,\quad \frac{r_{k+1}}{r_k}=\frac{r_k^2}{R_k^2}\ \exp\left[-\left(\frac{r_k^2}{2R_k^2}\right)\right].$$

Hence, introducing the variable $x_k=(r_k/R_k)^2(\gg 1)$, we obtain the recurrence equation

$$x_{k+1}=x_k^{-3}e^{x_k},$$

whence it is seen that x_k is an exponentially diverging sequence. In terms of x_k we have

$$r_{k+1}/r_k=x_k e^{-x_k/2}.$$

This ratio can be understood as the ratio of neighboring periods of the oscillations, since $r_k \gg r_{k+1}$. The values of the function $|\Delta|$ at the points r_k rapidly approach zero

$$|\Delta(r_k)|=x_k^{-1},$$

so that we are dealing with an infinite sequence of ''almost'' Cauchy horizons as $r\to 0$. At the same time, the values of $|\Delta|$ at the points R_k grow rapidly as

$$|\Delta(R_k)|=x_k^{-3/2}e^{x_k/2},$$

and, correspondingly, the values of the mass function grow as

$$M_k/M_{k-1}=x_k^{-1}e^{x_k/2}.$$

As shown in Ref. 3, in this regime the system (7) and (8) can be reduced to a two-dimensional dynamical system, one of whose singular points is an unstable focus with an infinitely untwisting phase trajectory.

As r decreases from r_k to R_k, the function σ decreases rapidly to the value $\sigma_k=\sigma(R_k)$ and then remains practically constant up to r_{k+1}. In the direction toward the singularity the sequence σ_k decreases according to the law

$$\sigma_{k+1}/\sigma_k=e^{-x_k/2}.$$

Let us now examine the structure of the singularity for black holes of general type in the EYMD theory. In this case, starting the numerical integration at the horizon, we do not encounter giant oscillations of the metric in the interior region. The general solution does not exhibit Cauchy horizons, so that Δ remains negative definite for all $0<r<r_h$. For sufficiently small r the right-hand sides of Eqs. (3)–(5) become small compared with the terms on the left-hand side, and we obtain the simplified system of equations

$$(\ln U)'-2\phi'=0, \quad [\ln(\Delta/r)]'=[\ln(\Delta\phi')]'=-r\phi'^2. \tag{16}$$

Integrating this system gives the following five-parameter (that is, of general form) solution

$$W=W_0+br^{2(1-\lambda)}, \quad \Delta=-2\mu r^{(1-\lambda^2)}, \quad \phi=c+\ln(r^{-\lambda}) \tag{17}$$

with the constants W_0, b, c, μ, and λ. The validity of the truncated equations (16) can now be checked by substituting the asymptotic solution (17) into the complete system (3)–(5). For consistency, it is sufficient that $\sqrt{2}-1<\lambda<1$, which is in agreement with the numerical data.

It follows from Eq. (17) that the mass function diverges according to a power law as $r\to 0$

$$m(r)=\mu r^{-\lambda^2}.$$

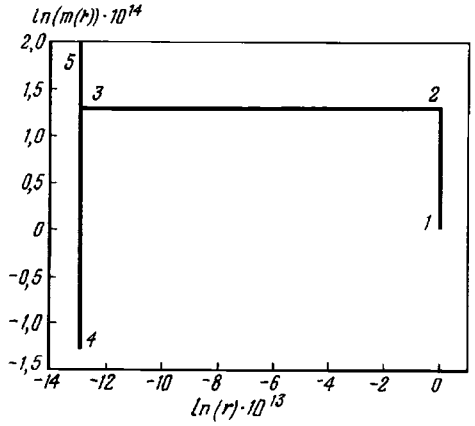

FIG. 2. Second oscillation of the mass function for the EYM system. The numbers indicate the order in which the curve is traversed as $r \to 0$. The parameters of the solution are the same as in Fig.1.

The dilaton diverges logarithmically, while the YM function W possesses a finite limit. The corresponding function σ approaches zero as

$$\sigma(r) = \sigma_1 r^{\lambda^2},$$

where $\sigma_1 =$ const.

The regimes described above correspond to the expectation that the singularity inside black holes of general form should be space-like. The metric (2) in the interior region of a black hole corresponds to the anisotropic cosmological Kantov–Sax solution. It can be shown that the corresponding deformation parameter $\tilde{\sigma}$, determining the deformation tensor $\sigma_{ij} = (2,-1,-1)\tilde{\sigma}/3$, grows infinitely as the singularity is approached. For the oscillating EYM solution the values of $\tilde{\sigma}$ at the points R_k are of the order of

$$\tilde{\sigma}_k^{\max} \sim M_k^{1/2}/R_k^{3/2},$$

while the values at the points r_k are of the order of

$$\tilde{\sigma}_k^{\min} \sim M_{k-1}/R_{k-1}.$$

Both sequences are infinitely growing. For the EYMD solution $\tilde{\sigma}$ diverges as a power law.

In summary, spherical non-Abelian black holes of *general type* correspond to the strong principle of cosmic censure (the singularity is space-like). In the case of the EYM theory, however, there is an infinite sequence of ''almost'' Cauchy horizons near which the mass function starts to grow exponentially, stabilizing at a value corresponding to the next cycle; the sequence of these values diverges exponentially as the singularity is approached. In the theory with a dilaton the mass function approaches infinity monotonically (in a power-law fashion). In the cosmological interpretation, this behavior of the matrix corresponds to an infinite growth of the anisotropy.

D. V. G. thanks the theoretical division of CERN for hospitality in December of 1996, when this work was in progress. This research was sponsored by the Russian Fund for Fundamental Research under Grants Nos. 96-02-18899 and 18126.

[a)]e-mail: galtsov@grg.phys.msu.su

---

[1] M. S. Volkov and D. V. Gal'tsov, JETP Lett. **50**, 346(1989); Yad. Fiz. **51**, 1171 (1990) [Sov. J. Nucl. Phys. **51**, 747(1990)]; H. P. Kunzle and A. K. M. Masood-ul-Alam, J. Math. Phys. (N.Y.) **31**, 928 (1990); P. Bizon, Phys. Rev. Lett. **64**, 2844 (1990).

[2] D. V. Gal'tsov and M. Yu. Zotov, ''Interior solution for Einstein–Yang–Mills black holes,'' in *Abstracts of Reports at the International School–Seminar ''Foundations of Gravitation and Cosmology''*[in Russian], Odessa, September 4–10, 1995, p. 16; ''New asymptotic solutions for the Einstein–Yang–Mills equations,'' in *Abstracts of Reports at the 9th Russian Gravitation Conference* [in Russian], Novgorod, July, 1996.

[3] E. E. Donets, D. V. Gal'tsov, and M. Yu. Zotov, ''Internal Structure of Einstein-Yang-Mills Black Holes,'' Preprint DTP-MSU/96-41,gr-qc/9612067.

[4] P. Breitenlohner, G. Lavrelashvili, and D. Maison, ''Mass inflation and chaotic behavior inside hairy black holes,'' MPI-PhT/97-20,gr-qc/9703047.

[5] J. A. Smoller and A. G. Wasserman,''Reissner-Nordström-like solution of the $SU(2)$ Einstein–Yang–Mills equations,'' gr-qc/9703062.

[6] D. V. Gal'tsov and E. E. Donets, Int. J. Mod. Phys. D **3**, 755 (1994).

Translated by M. E. Alferieff

Does the Unruh effect exist?

V. A. Belinskiĭ[a)]
INFN and ICRA, Rome University ''La Sapienza,'' 00185 Rome, Italy

B. M. Karnakov, V. D. Mur, and N. B. Narozhnyĭ[b)]
Moscow State Engineering-Physics Institute, 115409 Moscow, Russia

(Submitted 23 March 1997; resubmitted 23 May 1997)
Pis'ma Zh. Éksp. Teor. Fiz. **65**, No. 12, 861–866 (25 June 1997)

It is shown that quantization on the Fulling modes presupposes that the field vanishes on the spatial boundaries of the Rindler manifold. For this reason, Rindler space is physically unrelated with Minkowski space and the state of a Rindler observer cannot be described by the equilibrium density matrix with the Fulling–Unruh temperature. Therefore it is pointless to talk about an Unruh effect. The question of the behavior of an accelerated detector in the physical formulation of the problem remains open. © *1997 American Institute of Physics.* [S0021-3640(97)00212-0]

PACS numbers: 03.70.+k, 04.60.−m

1. According to Unruh,[1] a detector moving with uniform acceleration in a flat space-time detects particles even in vacuum. More precisely, the Unruh effect means that a Rindler (uniformly accelerated) observer is located in a heat bath with the Fulling–Unruh temperature

$$T=\frac{g}{2\pi}, \tag{1}$$

where g is the constant acceleration measured in a comoving reference frame ($\hbar=c=1$). It is also asserted[1–6] that for a Rindler observer the vacuum state in Minkowski space (MS) is described by a density matrix with the temperature (1). By analogy to the Hawking effect,[7] this is a fundamental problem. For brevity, this letter discusses the problem for the example of a massive scalar field in two-dimensional space-time. The extension to the four-dimensional case is made directly by introducing transverse (with respect to the direction of motion of a Rindler observer) components of the momentum **q** and making the substitution $m\to(m^2+q^2)^{1/2}$ (see, for example, § 12.1 in Ref. 5).

2. The geometry of Rindler space (RS) is described by the metric $ds^2=\rho^2 d\eta^2-d\rho^2$, $-\infty<\eta<\infty$, $\rho\geqslant 0$. The variables in the Klein–Fock–Gordon (KFG) equation

$$\left(\frac{\partial^2}{\partial\eta^2}+G(\rho)\right)\phi_R(x)=0,\quad G(\rho)=-\rho\frac{\partial}{\partial\rho}\rho\frac{\partial}{\partial\rho}+m^2\rho^2,\quad x=\{\eta,\rho\}, \tag{2}$$

separate, and for the positive-frequency (with respect to the time coordinate η) solutions $\Phi_\mu(x)$, the Fulling modes,[8] we have

$$\Phi_\mu(x)=\pi^{-1}(\sinh(\pi\mu))^{1/2}K_{i\mu}(m\rho)e^{-i\mu\eta},\quad \mu>0, \tag{3}$$

where $K_\nu(y)$ is a Macdonald (modified Bessel) function. These modes are orthogonal relative to the scalar product in RS:

$$(\Phi_\mu,\Phi_{\mu'})_R\equiv i\int_0^\infty \frac{d\rho}{\rho}\Phi_\mu^*(x)\overleftrightarrow{\frac{\partial}{\partial\eta}}\Phi_{\mu'}(x)=\delta(\mu-\mu') \tag{4}$$

and form (together with $\Phi_\mu^*(x)$) a complete system of solutions of the KFG equation. They can be used as a basis for quantizing the field ϕ_R

$$\phi_R(x)=\int_0^\infty d\mu(c_\mu\Phi_\mu(x)+c_\mu^+\Phi_\mu^*(x)),\quad [c_\mu,c_{\mu'}^+]=\delta(\mu-\mu'), \tag{5}$$

and to determine the vacuum in Rindler space by the relation $c_\mu|0_R\rangle=0$, $\mu\geqslant 0$:

$$c_\mu=(\Phi_\mu,\phi_R)_R=\frac{i}{\pi}(\sinh(\pi\mu))^{1/2}\int_0^\infty\frac{d\rho}{\rho}K_{i\mu}(m\rho)\left[\frac{\partial\phi_R(\eta,\rho)}{\partial\eta}-i\mu\phi_R(\eta,\rho)\right]_{\eta=0}. \tag{6}$$

The differential operator $G(\rho)$, whose eigenfunctions are solutions of Eq. (3), operates in the Hilbert space of the single-particle states with scalar product $\langle\chi,\psi\rangle=\int_0^\infty(d\rho/\rho)\,\chi^*\psi$. It is easily verified that the hermiticity of this operator, ensuring completeness and orthogonality of the modes (3), presumes that the boundary condition

$$\phi_R(\eta,0)=0 \tag{7}$$

is satisfied. When this condition holds, the integral in Eq. (6) converges absolutely and the quantities c_μ^+ and c_μ are particle creation and annihilation operators. When the condition (7) does not hold, the integral in Eq. (6) can still be given a formal meaning, but in this case the c_μ become singular as $\mu\to 0$. This leads to divergences in the expressions for physical quantities, so that c_μ^+ and c_μ cannot be interpreted as particle creation and annihilation operators. Specifically, if $\phi_R(\eta,0)=$ const $\neq 0$, then the Rindler-quantum number operator $N_R=\int_0^\infty c_\mu^+c_\mu d\mu$ does not exist.

We note that the change of variables $\rho=e^u$, mapping the point $\rho=0$ into $u=-\infty$, reduces the requirement (7) to the standard condition for vanishing of the field ϕ_R at spatial infinity.

3. The change of variables

$$t=\rho\sinh\eta,\quad z=\rho\cosh\eta \tag{8}$$

leads to the Minkowski metric $ds^2=dt^2-dz^2$. Global coordinates$\{t,z\}$ are defined in all MS, while the Rindler coordinates $\{\eta,\rho\}$ cover only one sector of MS (Rindler wedge). We note that the Jacobian of the transformation (8) $J=\rho$ vanishes at the boundary of this wedge (in the two-dimensional case — on the light cone $z^2-t^2=0$).

Since the world line $z^2-t^2=g^{-2}$ of a uniformly accelerated observer in MS is also an orbit of Lorentzian rotations, we shall examine the eigenfunctions of the boost generator which have the integral representation[9] ($-\infty<\kappa<\infty$):

$$\Psi_\kappa(x)=2^{-3/2}\pi^{-1}\int_{-\infty}^{\infty}d\theta\,\exp\{-i[m(t\,\cosh\,\theta-z\,\sinh\,\theta)+\kappa\theta]\}. \tag{9}$$

It is easy to verify that these modes are ortho normalized with respect to the standard scalar product $(\phi,\psi)_M$ in MS, they form a complete system of solutions of the KFG equation, and they can be used as a basis for second quantization:[c)]

$$\phi(x)=\int_{-\infty}^{\infty}d\kappa[b_\kappa\Psi_\kappa(x)+b_\kappa^+\Psi_\kappa^*(x)],\quad [b_\kappa,b_{\kappa'}^+]=\delta(\kappa-\kappa'). \tag{10}$$

The operators b_κ are in a one-to-one relation with the operators a_p determined in a plane-wave basis, $\Psi_p=(4\pi\epsilon)^{-1/2}\exp(-i\epsilon t+ipz)$, $\epsilon=(p^2+m^2)^{1/2}$, and

$$b_\kappa=\int_{-\infty}^{\infty}dp(2\pi\epsilon)^{-1/2}\exp\left(i\frac{\kappa}{2}\ln\frac{p_+}{p_-}\right)a_p,\quad p_\pm=\epsilon\pm p. \tag{11}$$

Hence one can see that the solutions $\Psi_\kappa(x)$ correspond to positive frequencies relative to global time t, and for the Minkowski vacuum we have $b_\kappa|0_M\rangle=0$, $-\infty<\kappa<\infty$.

Introducing the null coordinates $x_\pm=t\pm z$, we can represent the modes (9) in the form

$$\Psi_\kappa(x)=\theta(x_+)\,\theta(-x_-)\Psi_\kappa^R+\theta(x_+)\,\theta(x_-)\Psi_\kappa^F+\theta(-x_+)\,\theta(x_-)\Psi_\kappa^L$$
$$+\theta(-x_+)\,\theta(-x_-)\Psi_\kappa^P, \tag{12}$$

corresponding to separation of Minkowski space into right-hand (R), future (F), left-hand (L), and past (P) sectors. For the functions Ψ_κ^R we have

$$\Psi_\kappa^R=2^{-1/2}\pi^{-1}K_{i\kappa}(m(-x_-x_+)^{1/2})\exp\left[-i\frac{\kappa}{2}\left(\ln\frac{x_+}{-x_-}+i\pi\right)\right]. \tag{13}$$

The remaining functions are obtained hence via the substitution $-x_\pm\to e^{i\pi}x_\pm$. More accurately, the modes (9) are analytical continuations of the functions (13), and traversing a circuit about the branch points $x_\pm=0$ we have $(-x_-)\to x_-e^{i\pi}$, $x_+\to(-x_+)e^{-i\pi}$, $x_-\to(-x_-)e^{-i\pi}$, and $(-x_+)\to x_+e^{i\pi}$ with the transitions $R\to F$, $F\to L$, $L\to P$ and $P\to R$, respectively. The substitution $-x_\pm\to x_\pm e^{-i\pi}$ gives a second independent choice of the solutions Ψ_κ^*.

The branch points merge at $t=0$. Therefore, to express the operators b_κ in terms of the values of the field ϕ and its derivatives on the Cauchy surface $t=0$ they must be calculated at $t\neq0$ and the limit $t\to0$ taken. Finally, we have

$$b_\kappa=(\Psi_\kappa,\phi)_M=\frac{ie^{\pi\kappa/2}}{\pi\sqrt{2}}\int_0^\infty F_R(z,\kappa)dz+\frac{ie^{-\pi\kappa/2}}{\pi\sqrt{2}}\int_{-\infty}^0 F_L(z,\kappa)dz, \tag{14}$$

where

$$F_{R,L}(z,\kappa)=K_{i\kappa}(\pm mz)\left(\frac{\partial\phi}{\partial t}\mp\frac{\partial\phi}{\partial z}\right)_{t=0}+\Gamma(-i\kappa)\left(\pm\frac{mz}{2}\right)^{\pm i\kappa}\frac{\partial\phi}{\partial z}\bigg|_{t=0}$$
$$+m\left[K_{i\kappa\mp1}(\pm mz)-\frac{1}{2}\Gamma(1\mp i\kappa)\left(\pm\frac{mz}{2}\right)^{\pm i\kappa-1}\right]\phi(0,z)$$

(the upper (lower) signs correspond to the indices R (L)). Here it is assumed that the field ϕ decreases quite rapidly at spatial infinity, but in contrast to Eq. (6) the condition $\phi(0,z)=0$ need not be satisfied at $z=0$.

4. Instead of the solutions (9), Unruh proposed using right-hand $R_\mu(x)$ and left-hand $L_\mu(x)$ modes such that $R_\mu(x)=0$ in the$L$ sector and $L_\mu(x)=0$ in the R sector. In the case at hand these are the functions

$$\begin{aligned}R_\mu(x)&=(2\sinh(\pi\mu))^{-1/2}[e^{\pi\mu/2}\Psi_\mu(x)-e^{-\pi\mu/2}\Psi^*_{-\mu}(x)],\quad \mu>0,\\ L_\mu(x)&=(2\sinh(\pi\mu))^{-1/2}[e^{\pi\mu/2}\Psi^*_{-\mu}(x)-e^{-\pi\mu/2}\Psi_\mu(x)],\quad \mu>0,\end{aligned}\tag{15}$$

satisfying the KFG equation and ortho normalized with respect to the scalar product in MS: $(R_\mu,R_{\mu'})_M=-(L_\mu,L_{\mu'})_M=\delta(\mu-\mu')$, $(R_\mu,L_{\mu'})_M=0$. Inverting the relations (15) and substituting the result into the expansion (10), we obtain[1–6]

$$\phi=\int_0^\infty d\mu[r_\mu R_\mu(x)+r^+_\mu R^*_\mu(x)+l_\mu L^*_\mu(x)+l^+_\mu L_\mu(x)],\tag{16}$$

where

$$\begin{aligned}r_\mu&=(2\sinh(\pi\mu))^{-1/2}[e^{\pi\mu/2}b_\mu+e^{-\pi\mu/2}b^+_{-\mu}],\quad \mu>0,\\ l_\mu&=(2\sinh(\pi\mu))^{-1/2}[e^{\pi\mu/2}b_{-\mu}+e^{-\pi\mu/2}b^+_\mu],\quad \mu>0,\end{aligned}\tag{17}$$

and $[r_\mu,r^+_{\mu'}]=[l_\mu,l^+_{\mu'}]=\delta(\mu-\mu')$. Hence follows

$$\langle 0_M|r^+_{\mu'}r_\mu|0_M\rangle=(e^{2\pi\mu}-1)^{-1}\delta(\mu-\mu').\tag{18}$$

The operators r_μ are expressed as a scalar product in MS: $r_\mu=(R_\mu,\phi)_M$. If here the surface $t=0$ is taken as the surface of integration and the fact that the modes $R_\mu=0$ for $z<0$ and are functionally the same as the Fulling modes (3) for $z>0$ is taken into account, then after making the change of variables (8) it can be shown that $(R_\mu,\phi)_M=(\Phi_\mu,\phi)_R$. Then the operators r_μ are identified with c_μ, after which the equality (18) is converted to the part of the particle number which refers to the interval of the proper time $\tau=\eta/g$ of a Rindler observer

$$\frac{dN}{d\tau}=\int_0^\infty\frac{d\omega}{2\pi}[e^{2\pi\omega/g}-1]^{-1},\quad \omega=g\mu,\tag{19}$$

and interpreted as an Unruh effect, i.e., the presence (from the point of view of the Rindler observer) of particles with a Bose thermal spectral at temperature (1) in the Minkowski vacuum. However, such an interpretation[1–6] is inadmissable. Indeed, substituting relation (14) into the first of the equations (17) and making the change of variables (8), we obtain the relation

$$r_\mu = \tilde{c}_\mu + \frac{i}{2\pi}(\sinh(\pi\mu))^{1/2}\lim_{\rho\to 0}\left\{\phi(0,\rho)\left[\Gamma(-i\mu)\left(\frac{m\rho}{2}\right)^{i\mu} - \Gamma(i\mu)\left(\frac{m\rho}{2}\right)^{-i\mu}\right]\right\}, \tag{20}$$

where $\tilde{c}_\mu$ is determined by Eq. (6) after the substitution $\phi_R(x)\to\phi(x)$ has been made in it. It would make sense to separate the operator r_μ into two terms in accordance with the equation (20) only if the field ϕ vanishes at the origin of the MS. This requirement, necessary for the existence of the limit on the right-hand side of the equality (20), could be a consequence of the fact that the field ϕ satisfies some boundary condition on a space-like surface intersecting the Cauchy surface $t=0$ at $z=0$, and $\phi(0,0)=0$. However, such a boundary condition leads to the problem of quantizing the field $\tilde{\phi}$ with a Hamiltonian $\tilde{H}$, which is different from the problem of quantizing the free field ϕ in MS.

If $\phi_R(\eta,\rho)$ and $\phi(t,z)$ are identified with one another for $z=\rho>0$ and $t=\eta=0$, then the Schrödinger operator $\tilde{c}_\mu$ is identical to the operator c_μ determined by the equation (6). This identity is the basis of the proof of the Unruh ''effect.''[1–6] However, it is not legitimate to identify these operators with one another, since they refer to problems with different Hamiltonians. In contrast to the Hamiltonian H_R in RS, the Hamiltonian $\tilde{H}$ does not diagonalize even in terms of the operators r_μ and l_μ. Moreover, the operators $\tilde{H}$ and H_R are generators of evolution in global time t and in Rindler time η, respectively.

There are especially no grounds for identifying the operators r_μ given by the relations (17) in MS and the operators c_μ determined in the problem with the boundary condition (7). This condition corresponds to the presence of an impenetrable wall at $\rho=0$, $-\infty<\eta<\infty$, i.e., at the boundary of the Rindler manifold, so that RS is in no way physically related with MS. In consequence, the union of the two Cauchy surfaces $\eta=0$ in the left- and right-hand Rindler spaces, i.e., the surface $t=0$ in MS with the point $z=0$ excluded, is not a Cauchy surface in this space.

As an example for elucidating this assertion we give the function $D(t,z)=[\phi(x),\phi(0)]_-$, for which $D(0,z)=0$ and $(\partial/\partial t)D(t,z)|_{t=0}=\delta(z)$. This function is different from zero inside the light cone, though it possesses zero Cauchy data in both the R and L sectors. In four dimensions the well-known Pauli–Jordan function, which satisfies the KFG equation and the Cauchy initial data $D(0,\mathbf{r})=0$ and $(\partial/\partial t)D(t,\mathbf{r})|_{t=0}=\delta(\mathbf{r})$ and vanishes only outside the light cone, possesses similar properties. Therefore the assertion made above about the properties of the Cauchy surface is not specific to two dimensions.

Returning to relation (18), we underscore the fact that since $\omega=g\mu$ is not the energy in MS, since the average on the left-hand side is calculated over the Minkowski vacuum, and since the operators r_μ are defined in terms of the scalar product in MS, the expression $[e^{2\pi\omega/g}-1]^{-1}$ has nothing in common with a Bose distribution. Therefore $g/2\pi$ is not the temperature, and the Unruh effect in the sense (19) does not exist. The appearance of a Bose factor in Eq. (19) is entirely due to the specific properties of the Bogolyubov transformation (15) and is encountered in different physical problems where in no way does the question of temperature arise. An example is a two-dimensional oscillator.

The relation (18) is sometimes interpreted in terms of a density matrix. This interpretation is based on the formula[3,5]

$$\langle 0_M|\mathcal{R}(r_\mu, r^+_{\mu'})|0_M\rangle = \mathrm{Tr}_R(\rho_R \mathcal{R}),$$

$$\rho_R = \rho_0 \exp(-K_R/T), \quad K_R = \int_0^\infty \mu r^+_\mu r_\mu d\mu.$$

However, the development of the operators in Minkowski time is determined by the complete Hamiltonian and not by the operator K_R. Therefore the matrix ρ_R does not satisfy the dynamical Bloch equation and cannot be interpreted as a density matrix.

5. So, the problem of quantizing free fields is entirely different in Rindler and Minkowski spaces. Therefore analysis of these problems cannot serve as a basis for any conclusions about the behavior of an uniformly accelerated detector. The question of an accelerated detector is a very difficult fundamental problem and, in our opinion, does not have a satisfactory solution at present. Here we confine our attention only to brief remarks concerning it.

First, the problem of a Rindler observer and therefore a uniformly accelerated detector, discussed in Unruh's paper,[1] is to oidealized. Even in classical field theory, where the question of preparing a quantum state in which a measurement is performed does not arise, well-known paradoxes arise in the problem of hyperbolic motion of a charge.[11,12] Second, the use of composite systems[1] as a detector raises numerous questions, since at present a systematic relativistic theory of bound states does not exist. At the same time, the problem of the interaction of accelerated particles with quantized fields is urgent and has interesting physical applications; see, for example, Refs. 9 and 13. Specifically, it is shown in Ref. 9 that elementary particles used as detectors do not manifest the universal response of the Unruh type. The question of an accelerated detector must be discussed in a physically correct formulation with acceleration switched on and off and remains open at present. However, it is difficult for us to believe that the behavior of the detector will be universal and will follow Unruh's formula.

We thank S. E. Murav'ev for a discussion. We are especially grateful to A.A. Starobinskiĭ, who read through the manuscript and made many helpful remarks. One of us (N. B. N.) thanks Professor R. Ruffini for hospitality at Rome University. This work was supported in part by the Russian Fund for Fundamental Research under Projects Nos. 95-02-05417a and 95-02-06056a.

[a)]e-mail: volodia@vxrmg9.icra.it
[b)]e-mail:narozhny@theor.mephi.msk.su
[c)]The quantization of the scalar field performed previously in Ref. 10 by means of analytical continuation of the Green's functions is equivalent to quantization on the modes (9).

[1] W. G. Unruh, Phys. Rev. D **14**, 870 (1976).
[2] N. D. Birrell and P. C. W. Davies, *Quantum Fields in Curved Space*, Cambridge University Press, New York, 1982.
[3] W. Greiner, B. Müller, and J. Rafelski, *Quantum Electrodynamics of Strong Fields*, Springer-Verlag, New York, 1985.
[4] V. L. Ginzburg and V. P. Frolov, Usp. Fiz. Nauk **153**, 633 (1987) [Sov. Phys. Usp. **30**, 1073 (1987)].

[5] A. A. Grib, S. G. Mamaev, and V. M. Mostepanenko, *Vacuum Quantum Effects in Strong Fields* [in Russian], Énergoizdat, Moscow, 1988.
[6] R. M. Wald, *Quantum Field Theory in Curved Space-Time and Black Hole Thermodynamics*, Chicago University Press, Chicago, 1994.
[7] S. W. Hawking, Commun. Math. Phys. **43**, 199 (1975).
[8] S. A. Fulling, Phys. Rev. D **7**, 2850 (1973).
[9] A. I. Nikishov and V. I. Ritus, Zh. Éksp. Teor. Fiz. **94**, 31 (1988) [Sov. Phys. JETP **67**, 1313 (1988)].
[10] D. G. Boulware, Phys. Rev. D **11**, 1404 (1975).
[11] R. Peierls, *Surprises in Theoretical Physics*, Princeton University Press, Princeton, 1979.
[12] V. L. Ginzburg, *Theoretical Physics and Astrophysics*, Pergamon Press, New York, 1979 [Russian original, Nauka, Moscow, 1981].
[13] Ya. B. Zel'dovich, L. V. Rozhanskiĭ, and A. A. Starobinskiĭ, JETP Lett. **43**, 523 (1986).

Translated by M. E. Alferieff

Optical orientation in *p*-doped semiconductor structures with a split valence band

E. P. German and A. V. Subashiev[a)]
State Technical University, 195251 St. Petersburg, Russia

(Submitted 16 May 1997)
Pis'ma Zh. Éksp. Teor. Fiz. **65**, No. 12, 867–871 (25 June 1997)

The optical orientation of electron spins in heavily doped semiconductor structures with a valence band that is split as a result of size quantization or uniaxial deformation is investigated theoretically. It is shown that lowering the Fermi level by doping and by lowering the temperature should lead to sharp changes in the photon-energy-dependence of the average spin of the excited electrons in structures excited by circularly polarized light. This effect is due to an interchange of the dominant contribution of transitions from a light-hole subband and transitions from the heavy-hole subband in absorption. © *1997 American Institute of Physics.*
[S0021-3640(97)00312-5]

PACS numbers: 78.20.Bh, 73.20.Dx

Optical orientation in semiconductor structures is actively used both for studying the kinetics of non equilibrium states of electrons[1,2] and for producing efficient photoemitters with a high degree of polarization of the electron beam.[3] In strained semiconductor films (compressed in the plane of the hetero boundary) and in semiconductor structures with quantum wells, the degenerate Γ_8 state of the valence-band edge is split into doubly degenerate states with Γ_6 (heavy holes) and Γ_7 (light holes) symmetry, the heavy-hole subband having the higher energy (see Fig. 1). In the case when the electrons are excited by circularly polarized light near the absorption edge, the average projection of the electron spin on a direction opposite to that of the angular momentum of the exciting photon (which is oriented in the direction of the outer normal to the surface of the film) is found to be $S_z = 1/2$ and the polarization of the excited electrons is $P = 1$.

The spin orientation observed according to the luminescence polarization and the emission of polarized electrons reaches $P = 0.9$ for *p*-doped strained films[4] as well as in structures with quantum wells[5] and in superlattices.[6] For excitation energy above the threshold for excitation of transitions from light-hole states, the polarization P decreases rapidly, since electrons with opposite spin direction are produced in the case of excitation from the light-hole subband.

This letter analyzes of the optical orientation of electron spins in heavily doped *p*-type structures with a split valence band. At low temperatures the filling of the top hole subband with holes (downward displacement of the Fermi level), resulting in a shift of the absorption edge into the region of high energies, for sufficiently high hole density should lead to a change in the dominant mechanism of absorption, specifically, the edge

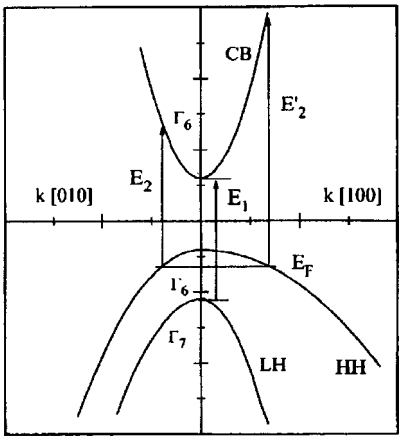

FIG. 1. Band structure scheme of a (100) GaAs film compressed in the(100) plane. The vertical lines show the thresholds of direct optical transitions from split light-hole (E_1) and heavy-hole (E_2,E_2') states in the valence band into states of the conduction band; E_F — Fermi level.

absorption should be determined by transitions from the split-off light-hole subband and not the heavy-hole subband. The edge-absorption mechanism changes when $E_F(1+m_{hh,\perp}/m_c)>\Delta$. Here E_F is the heavy-hole Fermi energy, m_c is the conduction-band effective mass, $m_{hh,\perp}$ is the transverse (with respect to the axis of the structure) effective mass in the heavy-hole subband, and Δ is the deformation splitting of the valence band. As the excitation energy increases, the contribution of heavy holes once again predominates in absorption.

This letter shows that in the case when the structure is excited by circularly polarized light a change of the dominant absorption mechanism should be accompanied by a sharp change in the average spin of the excited electrons, and this should be manifested as sharp changes in the polarization in the excitation spectra of the polarized luminescence and in the polarized-electron emission spectra. As the temperature increases, an upward shift of the Fermi level and broadening of the Fermi distribution cause the heavy holes to predominate in absorption and the standard spectral dependence of the electronic polarization is restored.

A similar ''inversion'' occurring in the spectral dependence of the electron polarization upon doping and lowering of the temperature should also be observed in structures with quantum wells and in superlattices as well as in heavily doped extended layers.

Let us consider the absorption of circularly polarized light in a strained *p*-GaAs layer oriented along the [100] axis. The number of electrons with ''upward'' (i.e., in a direction along the normal to the film) and''downward'' spin which are excited by light into the conduction band per unit time is determined (to within a factor) by the quantities[7]

$$\langle F^{\alpha}\rangle=\frac{2\pi}{\hbar V}\sum_{\mathbf{k},i} F_i^{\alpha} n(E_i(\mathbf{k}))\,\delta(E_c(\mathbf{k})-E_i(\mathbf{k})-\hbar\omega), \quad \alpha=\uparrow,\downarrow \tag{1}$$

Here $F_i^{\alpha}=\Sigma_m|\langle c,\alpha|e\hat{\mathbf{D}}|i,m\rangle|^2$, $i=h$ and l, the index m enumerates the states of the Γ_8 multiplet of the valence band, $E_{c,i}(\mathbf{k})$ are the energies of states with wave vector $\mathbf{k}$, $n(E_i(\mathbf{k}))$ is the Fermi distribution function of valence-band electrons, $\hat{\mathbf{D}}$ is the dipole-moment operator, $\mathbf{e}$ is the polarization vector of the light, and V is the volume of the crystal. Calculations of the quantities F_i^{α} (similar to the calculations performed in Ref. 7) give

$$F_{h,l}^{\uparrow}=\frac{1}{2}d^2(1\pm R),\quad F_{h,l}^{\downarrow}=\frac{1}{6}d^2(1\mp R), \tag{2}$$

where $d=\langle S|\hat{D}_x|X\rangle$ is an interband transition matrix element,

$$R=\frac{\tilde{\Delta}+2\gamma_2(3k_z^2-k^2)}{\sqrt{\tilde{\Delta}^2+2\gamma_2(3k_z^2-k^2)\tilde{\Delta}+4\gamma_2^2k^4+12(\gamma_3^2-\gamma_2^2)(k_x^2k_y^2+k_x^2k_z^2+k_y^2k_z^2)}}, \tag{3}$$

$\tilde{\Delta}=m_0\Delta/\hbar^2$, and γ_2 and γ_3 are the Luttinger parameters.

The absorption coefficient K and the degree of polarization P of the electrons are given by the equations

$$K=\frac{2\pi\hbar\omega}{cn}(\langle F^{\uparrow}\rangle+\langle F^{\downarrow}\rangle),\quad P=\frac{\langle F^{\uparrow}\rangle-\langle F^{\downarrow}\rangle}{\langle F^{\uparrow}\rangle+\langle F^{\downarrow}\rangle} \tag{4}$$

or

$$P=P_h\frac{K_h}{K_l+K_h}+P_l\frac{K_l}{K_l+K_h} \tag{5}$$

Here K_h and K_l are partial absorption coefficients and P_h and P_l are the degree of polarization with excitation of electrons from the light- and heavy-hole subbands, respectively. It follows from Eqs.(2)–(5) that R decreases monotonically with increasing electron energy, as a result of which P_h changes from 1 to 1/2 and P_l changes from -1 to 1/2. The resulting electronic polarization is determined by the relative contribution of transitions from the light- and heavy-hole subbands.

For optical excitation energy E, measured from the interband absorption threshold ($E=\hbar\omega-E_g$, E_g is the band gap in the strained layer), $E\leqslant(m_{h,\perp}/m_e)\Delta$, the effect of the fluting of the hole spectrum is small ($\propto(\gamma_3-\gamma_2)/\gamma_2E/(m_h/m_e\Delta)$) and in the region $E<\Delta_{so}$, where Δ_{so} is the spin-orbit splitting of the valence band, the dependences $K(E)$ and $P(E)$ in the strained GaAs layer can be found analytically. The computational results for $K(E)$ are displayed in Fig. 2 for several values of the hole density (the splitting is assumed to be $\Delta=30$ meV). One can see from Fig. 2 that as the hole density increases for densities $p\geqslant3\times10^{17}$ cm^{-3}, the absorption threshold shifts appreciably into the region of high energies.

We call attention to the square-root dependence (due to the anisotropy of the heavy-hole subband in the strained material) of the one-band absorption coefficients near the thresholds and the rapid growth (due to the relatively high density of states of the heavy

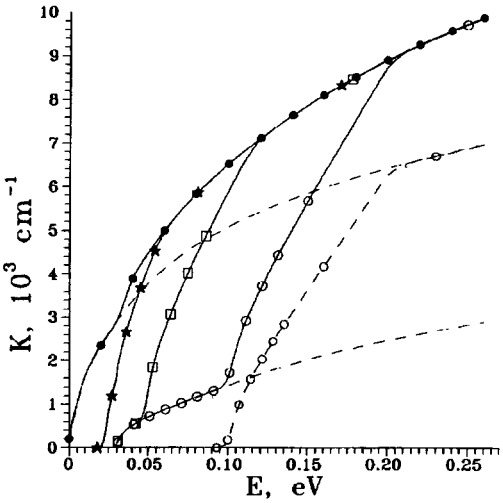

FIG. 2. Spectral dependence of the absorption coefficient in a doped strained GaAs layer at $T=4$ K: ● — $p=10^{17}$ cm^{-3}, ⋆ — $p=3\times10^{17}$ cm^{-3}, □ — $p=10^{18}$cm^{-3}, ○ — $p=3\times10^{18}$ cm^{-3}. The dashed lines show the partial contributions of the light-hole and heavy-hole subbands to absorption at low density and ○.

holes and the large optical matrix element) of the absorption at the edge of the transitions from the heavy-hole subband in the doped material. This increase becomese specially clear for $E_F>0.4\Delta$.

The dependence of the electronic polarization on the excitation energy attemperature $T=4$ K is shown in Fig. 3 for a series of hole densities. At low hole density the electronic polarization is high and positive right up to excitation energy equal to the deformation-

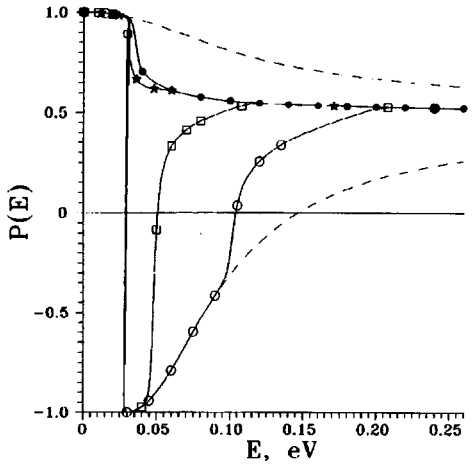

FIG. 3. Spectral dependence of the electron polarization $P(E)$. The symbols have the same meaning as in Fig. 2.

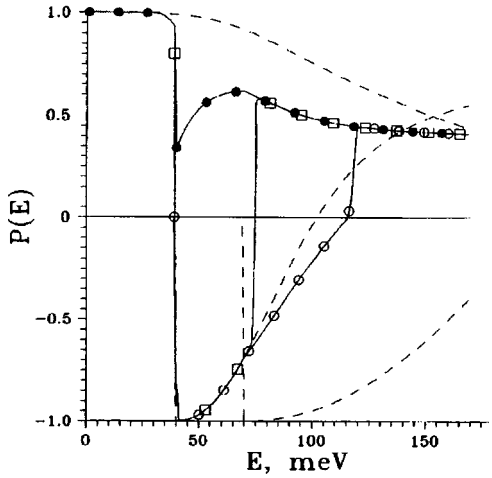

FIG. 4. Spectral dependence of the electron polarization $P(E)$ in adoped structure with a 5 nm wide GaAs quantum well at $T=4$ K; ●— $p=10^{11}$ cm^{-2}, □ — $p=10^{12}$ cm^{-2}, ○— $p=1.5\times10^{12}$ cm^{-2}. The dashed lines show the partial contributions of transitions from the $hh1$, $lh1$, and $hh2$ subbands.

splitting energy. For $p>5\times10^{17}$ cm^{-3} anomalously large changes arise in the electronic polarization in the region of low excitation energies and the width of the anomalous-polarization band increases with the hole density.

The calculations of the electronic polarization for smaller valence-band splitting and higher temperatures show that for strained GaAs films with $m_{hh,\perp}/m_c>1$ and typical values $\Delta\geqslant20$ meV, the anomalous behavior of the electronic polarization remains strongly expressed even for $T\leqslant77$ K and $p\geqslant10^{18}$ cm^{-3} .

The splitting of the spectrum in superlattices and structures with quantum wells is due to the formation of a collection of size-quantization subbands of hole states, and sharp changes in the electronic polarization are observed at the thresholds of interband transitions from the size-quantization hole subbands.[5,8] In this case also the calculation of the spectral dependence of the electronic polarization reduces to the calculation of the number of electrons which are excited into a state with the opposite spin orientation in the conduction band (see Ref. 9). However, this requires a numerical calculation of the size-quantization spectra of the electrons and holes and a calculation of the interband transition matrix elements and the density of final states. The computational results for the degree of electronic polarization of the electrons for a GaAs/$Ga_{0.7}Al_{0.3}As$ structure with 5-nm wide GaAs wells (in the model described in detail in Ref.10) are displayed in Fig. 4. For this structure the splitting between the first heavy-hole ($hh1$) and light-hole ($lh1$) subbands equals 40 meV, the $lh1$ subband having an anomalously large mass, which is also manifested in the form of a dip in the polarization spectrum. The anomalous-polarization band arises with two-dimensional hole density $p>6\times10^{11}$ cm^{-2}.

In contrast to the spectra of strained films, the spectral dependence of the polarization for quantum wells is very sensitive to the parameters of the structures (composition

and width of the layers), which change both the ratio between the partial absorption coefficients near the thresholds of the transitions between the size-quantization subbands $hh1-e1$, $lh1-e1$, and $hh2-e1$ and the order of the hole minibands.

The electron spin orientation is manifested in the circular polarization of the recombination radiation as well as in the polarization of the electrons emitted from a surface activated to negative electron affinity. In both cases the effects due to the spin relaxation processes can be eliminated by using time-resolved measurement techniques[11] and luminescence measurements with photon energy close to the excitation energy[12] (or by investigating energy-resolved emission[2]).This makes it possible to observe the predicted effect directly.

In view of its rapid variation, the above-predicted excitation-energy dependence of the electron polarization is very sensitive to the position of the Fermi level, Coulomb interaction effects, and fluctuation broadening of the absorption edge, all of which modify the carrier spectrum and the optical properties of doped structures.[13] For this reason, the observation of anomalous polarization and the determination of the energies corresponding to a change in the sign of the polarization can be used to obtain independent information about these effects.

This work was sponsored by CRDF under Grant RPI-351, INTAS under Grant No. 94-1561, and by the Russian Fund for Fundamental Research.

[a)]e-mail: arsen@tuexph.stu.neva.ru

---

[1] D. N. Mirlin and V. I. Perel', in *Spectroscopy of Nonequilibrium Electrons and Phonons*, V, edited by C. V. Shank and B. P. Zakharchenya, Elsevier Science, New York, 1992, p. 269.
[2] C. Herman, H.-J. Drouhin, G. Lampel *et al.*, in *Spectroscopy of Nonequilibrium Electrons and Phonons*, V, edited by C. V. Shank and B. P. Zakharchenya, Elsevier Science, New York, 1992, p. 135.
[3] *Proceedings of the Workshop on Photocathodes for Polarized Electron Sources for Accelerators*, SLAC-432, January, 1994.
[4] B. D. Oskotskij, A. V. Subashiev, and Yu. A. Mamaev, Phys. Low-Dim. Struct. **1/2**, 77 (1997).
[5] A. M. Vasil'ev, F. Daiminger, J. Straka *et al.*, Superlattices Microstruct. **13**, 97 (1993).
[6] T. Omori, Y. Kurihara, Y. Takeuchi *et al.*, Jpn. J. Appl. Phys. **33**, 5676 (1994).
[7] M. I. D'yakonov and V. I. Perel', Zh. Éksp. Teor. Fiz. **60**, 1954 (1971) [Sov. Phys. JETP **33**, 1053 (1971)].
[8] Yu. Mamaev, A. Subashiev, Yu. Yashin *et al.*, Phys. Low-Dim. Struct. **10/11**, 61 (1995).
[9] I. A. Merkulov, V. I. Perel', and M. E. Portnoĭ, Zh. Éksp. Teor. Fiz. **99**, 1202 (1990) [Sov. Phys. JETP **72**, 669 (1990)].
[10] L. G. Gerchikov, G. V. Rozhnov, and A. V. Sybashiev, Zh. Éksp. Teor. Fiz. **101**, 143 (1992) [Sov. Phys. JETP **74**, 77 (1992)].
[11] E. Perez, L. Muñoz, L. Vina *et al.*, in *Proceedings of the 23rd International Conference on the Semiconductor Physics*, Vol. 2, edited by M. Scheffler and R. Zimmerman, World Scientific, Singapore, 1996, p. 1975.
[12] V. F. Sapega, V. I. Perel', A. Yu. Dobin *et al.*, JETP Lett. **63**, 305 (1996).
[13] A. C. Ferreira, P. O. Holtz, I. Buyanova *et al.*, in *Proceedings of the 23rd International Conference on the Semiconductor Physics*, Vol. 2, edited by M. Scheffler and R. Zimmerman, World Scientific, Singapore, 1996, p. 1951.

Translated by M. E. Alferieff

Cluster structure and superlattices in Co and Fe films

S. M. Zharkov, V. S. Zhigalov, L. I. Kveglis, Yu. V. Lisitsa, K. V. Renskaya, and G. I. Frolov

L. V. Kirenskiĭ Institute of Physics, Siberian Branch of the Russian Academy of Sciences, 660036 Krasnoyarsk, Russia

(Submitted 29 April 1997)
Pis'ma Zh. Éksp. Teor. Fiz. **65**, No. 12, 872–875 (25 June 1997)

The process of dendritic crystallization of Co and Fe films is investigated. Electron-diffraction methods show that fractal growth of dendrites in Co and Fe films proceeds by multiple twinning of the elements of a nanostructure consisting of different clusters with close-packing. The formation of superstructures is explained by a shell model of a cluster structure forming nanocrystallites. © *1997 American Institute of Physics.* [S0021-3640(97)00412-X]

PACS numbers: 61.46.+w, 68.70.+w

In a previous work we presented electron-diffraction photographs obtained from iron films after explosive crystallization (EC) from an initial amorphous state. The electron-diffraction photographs did not correspond to either the α or γ phase of Fe, though they did contain a series of reflections from both phases. The hyperfine structure of the Mössbauer spectra of such films indicated the appearance of a new phase of Fe.[1] Investigations of the ferromagnetic characteristics of the Co and Fe films showed that in the course of dendritic growth the saturation magnetization decreases and the resistivity increases.[1,2]

In the present work we investigated Co and Fe films obtained by means of the same technology. The initial state of the films was x-ray amorphous. The films deposited on different substrates (LiFe, MgO, NaCl, glass) were subjected to multistep annealing in the temperature range from 50 to700 °C in a 10^{-5} torr vacuum. Explosive crystallization was observed under the action of an electron beam on films annealed at temperatures from 100 to 400 °C. The microstructure of the films consisted of a network of dendrites growing from centers of crystallization.

An electron-diffraction photograph of the dendritic section of a Co film is displayed in Fig. 1a. The main reflections in this photograph, taking account of twins, correspond to hcp-Co with a [110] zone axis.[3] Superstructural reflections, attesting to period doubling in the [002] and [012] directions, are also revealed in the electron-diffraction photograph.

Electron-diffraction photographs of three types of superlattices observed in iron films after explosive crystallization are displayed in Figs.1b, c, and d. An electron-diffraction photograph with two superstructural reflections between 0 and (211) α-Fe is displayed in Fig. 1b. These reflections can be attributed to multiple twinning along the (211) plane in α-Fe.[4] Figure 1c shows an electron-diffraction photograph containing not two but four and Fig. 1d shows six superstructural reflections between the central beam and the (211) α-Fe reflection. No correlation was found between the annealing tempera-

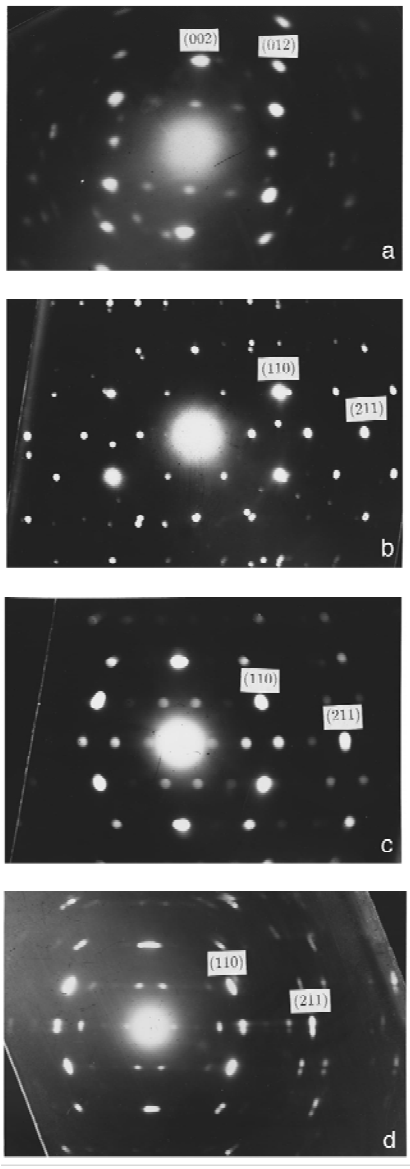

FIG. 1. Electron-diffraction photographs of Co (a) and Fe (b, c, d) films after explosive crystallization.

ture, the choice of substrate, and the type of superlattice; annealing only initiated the electron crystallization process. Relaxation of the structure and the physical properties of the films to the values characteristic for the bulk state started at anannealing temperature above 450 °C.

On the basis of the interpretation of electron-diffraction photographs, we can assume that multiple twinning leads to the appearance of superstructural reflections in Co and Fe

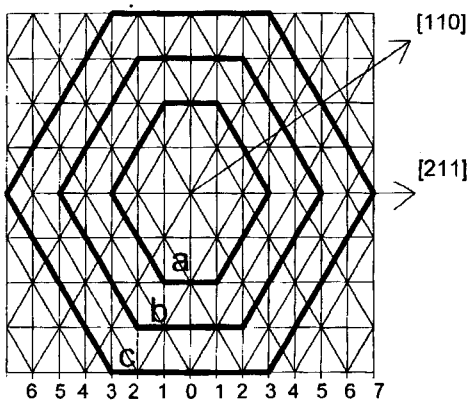

FIG. 2. Diagram of nanostructure formation. The thick lines distinguish the projections of a cubo-octahedron, when it is inscribed in a system of 7 (a), 11 (b), and 15 (c) (211)-type atomic planes. The numbered vertical lines show the traces of (211)-type planes.

films. Such twinning could result from the merging of nanocrystalline-size cubo-octahedron-shaped clusters. The appearance of superstructural reflections of the type (001) and$(0\frac{1}{2}1)$, associated with doubling of the corresponding periods in hcp-Co, is understandable if it is assumed that the clusters possess a close-packed ABAC-type structure characteristic for hcp-Co. An ABAC-type structure is an element of a cubo-octahedron.[5,6]

The dendritic growth process in iron films is identical to that in cobalt films. Figure 2 shows a diagram illustrating the appearance ofsuperstructural reflections in the electron-diffraction photographs of Fe films. The cubo-octahedral clusters increase in size during the annealing process. The initial equilateral cubo-octahedron is found to be inscribed in a system of seven parallel (211)-type planes (see Fig. 2a). Such a system of interatomic planes can form in an electron-diffraction photograph two superstructural reflections between the 0 and (211) reflections. If the cubo-octahedron inscribed in a system of 11 parallel planes of the type (211) (see Fig. 2b) is considered, then the reason why four superstructural reflections appear in the electron-diffraction photograph becomes understandable. The superstructure of a Fe film containing six superstructural reflections can be explained similarly if it is assumed that the cubo-octahedron is inscribed in asystem of 15 parallel (211)-type planes (see Fig. 2c).

It is well known that nanostructures can form in metal films obtained under ultra fast condensation conditions. In Ref. 7 the stability of clusters with different nanostructures (icosahedron, tetrahedron, octahedron, cubo-octahedron) was investigated theoretically as a function of the sizes of these clusters. It has been proved theoretically and experimentally[7,8] that the octahedra and cubo-octahedra are the most stable structures with dimensions exceeding 35 Å.

The well-known jellium model or shell model gives a quite accurate description of the stable structure of some elementary metal clusters.[9] In the jellium model, metal clusters are treated as giant macro atoms with electronic energy levels that manifest a

shell structure. The shell structure is similar to that determined for nuclei. The similarity to the nuclear model is observed experimentally. We suppose that the shell model can explain the discreteness of the volumes of the Co and Fe clusters.

According to the jellium model, an octahedron is the structural unit that possesses a closed resultant electronic shell consisting of six atoms. If it is assumed that the octahedron is the smallest unit in acubo-octahedron, then the decrease in the saturation magnetization in Co films[2] and Fe films[1] becomes understandable. When the structure of the film relaxes to an equilibrium structure on annealing, the saturation magnetization increases to a value characteristic of the bulk material.

The observed superlattices are a consequence of ordered intergrowth of clusters in the process of dendritic growth and illustrate the phenomenon of self-organization. On this basis, we consider it admissable to apply the cluster-structure model to explain the characteristic features of the physical properties of Co and Fe films.

[1] G. I. Frolov, O. A. Bayukov, V. S. Zhigalov *et al.*, JETP Lett. **61**, 63 (1995).
[2] L. I. Kveglis and Yu. V. Lisitsa, Poverkhnost' **8**, 5 (1996).
[3] P. B. Hirsch, A. Howie, R. B. Nicholson, D. W. Pashley, and M. J. Whelan [Eds.], *Electron Microscopy of Thin Crystals*, Plenum Press, New York, 1965 [Russian translation, Mir, Moscow, 1968].
[4] L. M. Utevskiĭ, *Diffraction Electron Microscopy in Materials Science*, [in Russian], Metallurgiya, Moscow, 1973.
[5] B. M. Smirnov, Usp. Fiz. Nauk **162**(12), 97 (1992) [Sov. Phys. Usp. **35**, 1052 (1992)].
[6] A. R. Verma and P. Krishna, *Polymorphism and Polytropism in Crystals*, Wiley, New York, 1966 [Russian translation, Mir, Moscow, 1969].
[7] Sh. Ino, J. Phys. Soc. Jpn. **27**, 941 (1969).
[8] Ch. Hayashi, Phys. Today **40**(12), 44 (1987).
[9] M. L. Cohen and W. D. Knight, Phys. Today **43**(12), 42 (1990).

Translated by M. E. Alferieff

Shift of the dip in the ultralow-frequency electric excitation spectrum of the Bridgman effect

E. G. Fateev[a)]

Institute of Applied Mechanics, Ural Branch of the Russian Academy of Sciences, 426001 Izhevsk, Russia

(Submitted 9 April 1997; resubmitted 14 May 1997)
Pis'ma Zh. Éksp. Teor. Fiz. **65**, No. 12, 876–880 (25 June 1997)

The previously predicted frequency shift of the deep dip in the ultra low-frequency (ULF) electric spectrum of the excitation threshold of the Bridgman effect in crystal hydrates has been observed. The appearance of this shift, which is caused by an increase in the temperature, is demonstrated for the example of magnesium hydroxide. The magnitude of the shift estimated qualitatively for two temperature — 20 °C and 180 °C — in a model with ULF-selective breakdowns of gas located in microcracks is virtually identical to the experimentally obtained value. This agreement attests to the possibility that micro breakdowns are excited in crystal hydrates under the conditions of a giant increase in their ULF permittivity in the process of strongly nonuniform quasistatic compression in relatively weak ac fields ($E<2$kV/cm). © *1997 American Institute of Physics.* [S0021-3640(97)00512-4]

PACS numbers: 62.50.+p, 77.22.Ch

1. INTRODUCTION

The Bridgman effect[1–3] is an explosive instability arising in almost all solid dielectrics and many semiconductors under strong uniaxial quasistatic compression ($dP/dt\sim 10^{-2}-1$ GPa/s) at high pressure ($P<10$ GPa). This phenomenon is accompanied by the ejection of some of the sample material out from the anvils in a microdisperse fractured form with velocities $v\sim 0.5-2$km/s, the excitation of shock waves in the compression system, an energetic pulse of electromagnetic radiation in a wide spectrum right up to the x-ray range,[4] as well as the emission of electrons[5] and possibly neutrons.[6,7] Radical structural changes occur in solids under Bridgman effect conditions[8–10] and intense interactions occur in mixtures of chemical reagents (see, for example, Ref. 11). It is known that the threshold P_c (or the average critical pressure in the body at which the Bridgman effect occurs in a given material) drops with increasing temperature and compression rate,[12] it is correlated with the thermodynamic parameters of materials, and it exhibits a dimensional dependence.[13]

It has recently been discovered in experiments with crystal hydrates[14–17] that quite weak ultralow-frequency (ULF) ($10<\omega_1<100$ Hz) and low-frequency (LF) ($10^2<\omega_2<10^6$ Hz) electric fields (with intensity $E<2$ kV/cm) strongly influence the excitation threshold P_c of the Bridgman effect. This phenomenon is of interest because of the global prevalence of crystal hydrates in the lithosphere (under high pressures and temperatures) and the possibility that only ULF electromagnetic waves penetrate into the

lithosphere. It has turned out that the frequency spectrum $P_c(\omega)$ for crystal hydrates possesses a single narrow deep dip (a decrease of the threshold by a factor of 1.5–2) in the frequency range $20<\omega_1<40$ Hz and a second wider dip near $\omega_2\sim10^4$ Hz. It has been shown that the depth $\Delta P(U)=P_c(U=0)-P_c(U)$ of the dip in the threshold as a function of the amplitude U of the ULF and LF voltage pulses increases as $\Delta P(U)\propto U^2$. For $U\approx65$ V and sample thicknesses $\sim0.3-0.8$ mm the ratios $\Delta P/P_c\sim0.5$ are common.

A special experiment performed in Ref. 14 made it possible to attribute the appearance of dips in the spectrum $P_c(\omega)$ in the LF region to heating due to dielectric losses. The dip in the spectra $P_c(\omega)$ at ULF frequencies is explained less trivially.[16] It follows from two, not mutually exclusive, models for these effects that the dips in the region $20<\omega_1<40$ Hz are caused by frequency-selective input of electric energy into breakdown; this input of energy is a consequence of a giant increase in the dielectric permittivity at ULF frequencies[16,17] in crystal hydrates which become partially dehydrated under strongly nonuniform compression. There exist definite methodological difficulties, which are described in Ref. 16, that make it impossible to record directly such ULF selective breakdowns, which evidently can be excited in $\sim10^3$ times weaker external fields than are ordinarily required for breakdown of crystal hydrates.[18] In consequence, the models proposed in Ref. 16 for the effect being described must be treated with caution. However, it follows from the models that the minimum in the ULF spectrum $P_c(\omega)$ can shift to the left or right along the frequency axis, depending on various factors that can affect crystal hydrates. This letter presents for the example of natural magnesium hydroxide (brucite) $Mg(OH)_2$ experimental evidence of the existence of a shift of the dip in the ULF spectrum $P_c(\omega)$ accompanying a change in the sample temperature.

2. EXPERIMENTAL ARRANGEMENT AND RESULTS

The ULF electric spectrum $P_c(\omega)$ for brucite was found by the same procedure as the one used for the model compounds $NH_4C_2O_4\times H_2O$ and $H_2C_2O_4\times 2H_2O$ (Refs. 14–16). The only difference was that the brucite samples were placed between Bridgman anvils (with VK-8 super hard alloy inserts with 5 mm in diameter working surfaces) not in the form of powder but rather in the form of small, ≈1 mm thick, monolithicingots, just as in Ref. 17. The temperature of the samples was changed right up to 180 °C through the Bridgman anvils, heated with special disk-shaped heating elements (3 mm thick) with the same diameter as the anvils. The samples compressed between the anvils up to average pressures $P\sim0.1P_c$ were heated up to $T\sim180$ °C after which they were subjected to strong quasistatic compression (at the rate $dP/dt\approx10^{-1}$ GPa/s) up to excitation of the Bridgman effect. The temperature was monitored with a thermocouple, the junction of which was brought directly to the working face of the ultrahand anvil case near the sample. Each point in the spectrum was the result of 10–15 explosions. Brucite was chosen for the present investigation because of the fortunate combination of some of its physical properties. For example, in contrast to the model compounds, in brucite the second elastic stage under uniaxial compression (necessary condition for the appearance of the Bridgman effect) exists in the entire required temperature range from 20 °C up to 200 °C. A reliable spectrum $P_c(\omega)$ from brucite for 20 °C can be obtained even for the high pressures $P\leqslant5.5$ GPa which are accessible for such experiments.[16]

As a result of these experiments, a deep dip, whose bottom was found to lie near

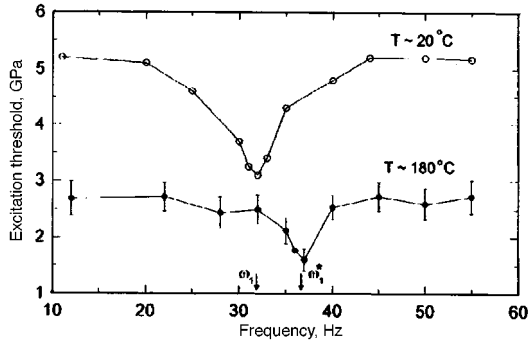

FIG. 1. Ultralow-frequency electric spectra $P_c(\omega)$ of the excitation threshold of the Bridgman effect in $Mg(OH)_2$ crystal hydrate($U=65$ V) at temperatures 20 °C (○) and 180 °C (●). The arrows mark the location of the bottom of the dips in the spectra $P_c(\omega)$ on the frequency axis for two temperatures.

$\omega_1^\star \sim 36-37$ Hz, as shown in Fig. 1, was found in the ULF spectrum $P_c(\omega)$ for brucite at the temperature $T\sim 180$ °C. The same figure shows for comparison a similar spectrum with a deep dip, found in Ref. 17, near $\omega_1 \sim 31-32$ Hz for brucite at $T\sim 20$ °C. We note that in both cases the samples were prepared from the same batch of natural brucite. Furthermore, an additional check of the form of the ULF spectrum $P_c(\omega)$ was made for this crystal hydrate at $T\sim 20$ °C in the region $30<\omega_1<35$ Hz. This check led to the same results as in Ref. 17. Therefore, when the temperature of the brucite samples is changed to $T\sim 180$ °C, the bottom of the minimum in the ULF spectrum $P_c(\omega)$ shifts rightward by $\Delta\omega\sim 5$ Hz along the frequency axis and the stability threshold P_c decreases by a factor of 2 at all ultralow frequencies. However, the latter circumstance for solids in the second elastic stage under strong uniaxial compression[19] can be easily explained on the basis of the thermal fluctuation theory of strength.[14]

In addition, the ULF dispersion of the permittivity $\epsilon(\omega)$ of brucite was investigated in order to elucidate the nature of the appearance of the shift of the dip in the ULF spectrum $P_c(\omega)$ under uniaxial compression conditions in brucite at $T\sim 180$ °C (the measurement procedure is described in Refs. 16 and 17). The frequency dependence $\epsilon(\omega)$ obtained in this experiment is shown for comparison with a similar curve[17] at $T\sim 20$ °C in Fig. 2. We note here that the giant values in the ULF dispersion of $\epsilon(\omega)$ in brucite under uniaxial compression conditions are maintained for tens of seconds $\Delta t \geqslant 10-50$ s, while in the model compounds they occur only in the form of a brief splash for $\Delta t \leqslant 1-2$ s.[16,17]

3. DISCUSSION AND CONCLUSIONS

Since in the first model of ULF dips with percolation intergrowth of breakdown[16] the giant splash in the ULF permittivity $\epsilon(\omega)$ under strong compression was assumed to be of short duration, $\Delta t \leqslant 1-2$ s, it is more correct to use the second model to describe the results obtained with $\Delta t \geqslant 10-50$ s. In accordance with the model of dips in the spectra $P_c(\omega)$ with breakdown of the gas in microcracks, the effective density of the electrical energy fed into plasma breakdown is found to have the frequency dependence[16,17]

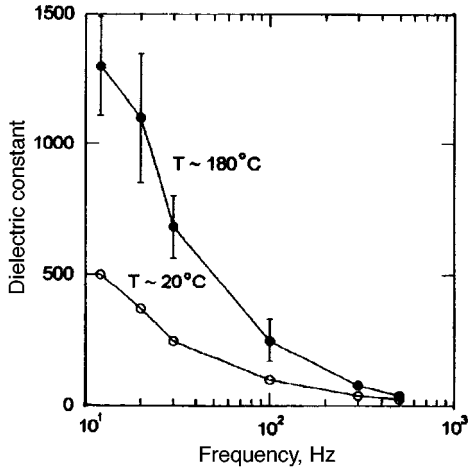

FIG. 2. Ultralow-frequency dispersion of the permittivity $\epsilon(\omega)$ at the moment of maximum growth under strong uniaxial compression of the hydrate crystal $Mg(OH)_2$ (for $U=65$ V) at temperatures 20 °C (○) and 180 °C (●).

$$w_{\text{eff}}(\omega)\propto(U/d)^2\epsilon^3(\omega)[1-\exp(-t_{\text{sp}}A/\epsilon(\omega))], \tag{1}$$

where $t_{\text{sp}}\propto\epsilon(\omega)^{-1}$ is the characteristic formation time of a spark discharge, U is the amplitude of the voltage pulses, and d is the thickness of the sample. For definite values of the parameter $A\propto n_0 e\mu$, reflecting the characteristics of the ionized gas in a microcrack (n_0 is the density, μ is the mobility, and e is the charge of the particles), the relation (1) has a maximum at ULF frequencies. It is assumed that the input of the maximum energy into the plasma discharge produces the strongest shock waves in microcracks, which is the main reason why the mechanical stability of crystal hydrates decreases and a deep dip appears in the ULF spectrum $P_c(\omega)$. The Debye equation $\epsilon(\omega)=\epsilon_\infty+(\epsilon_s-\epsilon_\infty)[1+(\omega\tau)^2]^{-1}$ is sufficient to find the qualitative behavior of $w_{\text{eff}}(\omega)$. Here ϵ_s is the maximum ULF permittivity, ϵ_∞ is the high-frequency permittivity, and τ is the relaxation time of the bound charges. In dispersed systems with electrical double layers (according to the models of Refs.15–17, crystal hydrates are in such a state during the partial-dehydration process), the relaxation time with dispersed particles of characteristic size a and volume diffusion coefficient D of the ions in the layers is determined from the relation $\tau=a^2/2D$ (Ref. 20). Setting $D=D_0\exp(-Q/kT)$, we find from the relation (1) that as the temperature increases, the sharp peak in the spectrum $w_{\text{eff}}(\omega)$ shifts rightward (Fig. 3). Here Q is the activation energy, k is Boltzmann's constant, and D_0 is a constant. The values of Q, D_0, and a (see caption to Fig. 3) employed for the calculation are typical for disperse systems.[20] The values of U, d, ϵ_∞, and ϵ_s were taken from experiments. The parameter A was obtained by matching, since it cannot be determined directly. If polynomials approximating the experimental curves $\epsilon(\omega)$ for two temperatures 20 °C and 180 °C (Fig. 2) are used instead of the Debye equation, then a shift of the maximum in the spectrum $w_{\text{eff}}(\omega)$ to higher frequency also follows from the relation (1).

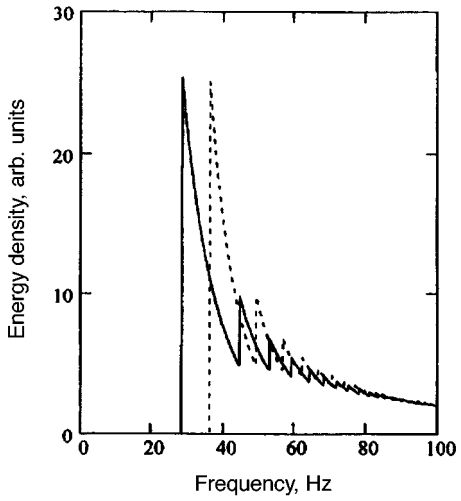

FIG. 3. Ultralow-frequency spectra of the effective energy density $w_{\text{eff}}(\omega)$ that can be put into ULF selective breakdown, as follows from the relation (1), for temperatures 20 °C (solid line) and 180 °C (dotted line). The spectra were found for the following values of the parameters: $A=10^{-11.5}$; $D_0=3\times10^{-7}$ m^2/s; $Q\leqslant10^{-22}$ J; $a=10^{-4}$ m; $\epsilon_\infty=6$; $\epsilon_s=500$ at 293 K; $\epsilon_s^*=1500$ at 453 K.

Therefore it definitely follows from the present work that the deep dip of the threshold of excitation of the Bridgman effect in crystal hydrates in a quite weak ULF electric field could be due to frequency-selective input of energy into breakdown of gas located in microcracks. Such breakdowns can evidently be excited by local breakdown fields which appear in the crystal hydrates as a result of the giant increase in the ULF dielectric permittivity accompanying the partial dehydration induced in the crystals by strongly nonuniform compression.

I am grateful to V. A. Aleksandrov for fabricating the components of the instrumentation, V. N. Avdonin for kindly providing the samples, and G. M. Mikheev for helpful discussions. This work was sponsored by the Russian Fund for Fundamental Research under Project No. 95-05-14488.

[a)]e-mail: fateev@ipm.udm.ru

[1] P. W. Bridgman, Phys. Rev. **48**, 825 (1935).
[2] P. W. Bridgman, Proc. Am. Acad. Art. Sci. **72**, 227(1938).
[3] P. W. Bridgman, *Studies in Large Plastic Flow and Fracture with Special Emphasis on the Effects of Hydrostatic Pressure*, McGraw-Hill, New York, 1952.
[4] T. Ya. Gorazdovskiĭ, JETP Lett. **5**, 64 (1967).
[5] M. A. Yaroslavskiĭ, *Rheological Explosion* [in Russian], Nauka, Moscow, 1982.
[6] M. A. Yaroslavskiĭ, Dokl. Akad. Nauk SSSR **307**, 369 (1989) [Sov. Phys. Dokl. **34**, 637 (1989)].
[7] M. A. Yaroslavskiĭ, Dokl. Akad. Nauk SSSR **308**, 95 (1989) [Sov. Phys. Dokl. **34**, 813 (1989)].
[8] E. G. Fateev and V. P. Khan, Fiz. Goreniya Vzryva **2**, 70 (1992).
[9] E. G. Fateev, I. G. Polyakov, and V. P. Khan, Pisma Zh. Tekh. Fiz. **17**(20), 47 (1991) [Sov. Tech. Phys. Lett. **17**, 734 (1991)].
[10] A. I. Aleksandrov, É. É. Gasparyan, V. S. Svistunov *et al.*, Dokl. Akad. Nauk SSSR **314**, 648 (1990).

[11] N. S. Enikolopyan, Dokl. Akad. Nauk SSSR **302**, 630 (1988).
[12] E. G. Fateev and V. P. Khan, Pis'ma Zh. Tekh. Fiz. **17**(20), 51 (1991) [Sov. Tech. Phys. Lett. **17**, 736 (1991)].
[13] N. S. Enikolopyan, É. É. Gasparyan, and A. A. Khzardzhan, Dokl. Akad. Nauk SSSR **294**, 1151 (1987).
[14] E. G. Fateev, Pis'ma Zh. Tekh. Fiz. **19**(10), 48 (1993) [Tech. Phys. Lett. **19**, 313 (1993)].
[15] E. G. Fateev, Pis'ma Zh. Tekh. Fiz. **20**(20), 83 (1994) [Tech. Phys. Lett. **20**, 847 (1994)].
[16] E. G. Fateev, Zh. Tekh. Phys. **66**(6), 93 (1996) [Tech. Phys. **41**, 571 (1996)].
[17] E. G. Fateev, Dokl. Akad. Nauk **354**, 231 (1997).
[18] A. A. Vorob'ev and G. A. Vorob'ev, *Electric Breakdown and Fracture of Solid Dielectrics* [in Russian], Vysshaya Shkola, Moscow, 1966.
[19] V. I. Levitas, *Large Elastoplastic Deformations of Materials at High Pressures* [in Russian], Naukova Dumka, Kiev, 1987.
[20] T. L. Chelidze, A. I. Derevyanko, and O. D. Kurilenko, *Electric Spectroscopy of Heterogeneous Systems* [in Russian], Naukova Dumka, Kiev, 1977.

Translated by M. E. Alferieff

A contribution to the theory of ferromagnetism in the Hubbard model with degeneracy

R. O. Zaĭtsev
Kurchatov Institute Russian Science Center, 123182 Moscow, Russia

(Submitted 15 May 1997)
Pis'ma Zh. Éksp. Teor. Fiz. **65**, No. 12, 881–886 (25 June 1997)

The possibility of ferromagnetic ordering in a generalized Hubbard model taking account of degeneracy is studied for an infinite Hubbard energy. The existence region of ferromagnetism for electron density greater than 1 is determined. © *1997 American Institute of Physics.* [S0021-3640(97)00612-9]

PACS numbers: 75.10.Jm

The ferromagnetic properties of transition metals are best described by the Hubbard model[1] with a strong repulsion of d electrons in the same unit cell. The long-range part of the Coulomb interaction is assumed to be very small, since its role is compensated by the screening effect of the s electrons. The Hubbard energy is assumed to be the largest energy parameter (see, for example, Ref. 2) and infinite at the outset. If $s-d$ hybridization is neglected, then the magnetic properties of transition elements are determined mainly by the d-electron subband, whose width is expressed in terms of hopping integrals. For simplicity and clarity, in the case of cubic crystals, which is of interest to us, we shall employ a model with zero off-diagonal and the same diagonal hopping integrals

$$\hat{H}=-\sum_{\mathbf{r},\mathbf{r}',\sigma,\lambda;\mathbf{r}\neq\mathbf{r}'} t_\lambda(\mathbf{r}-\mathbf{r}')\hat{a}^+_{\mathbf{r},\sigma,\lambda}\hat{a}_{\mathbf{r},'\sigma,\lambda}-\sum_{\mathbf{r},\sigma,\lambda}[\mu+\sigma H]\hat{a}^+_{\mathbf{r},\sigma,\lambda}\hat{a}_{\mathbf{r},\sigma,\lambda}. \tag{1}$$

Here μ is the chemical potential; $\sigma=\pm$ is the spin index; H is the external magnetic field; the crystal index λ takes on three values ($\lambda=xy, yz, zx$) when the t_{2g} shell is filled or two values ($\lambda=3z^2-r^2, x^2-y^2$) when the e_g shell is filled.

It can be shown that for density less than ferromagnetism exists only in special cases, when the Fermi surface passes near van Hove-type singularities. This makes it possible to explain the existence of ferromagnetism in Ni; see, for example, Refs. 3 and 4.

This letter studies the conditions (not associated with the existence of van Hove singularities) under which ferromagnetism appears. The calculations are performed in a one-loop approximation for electron or hole density greater than 1.

1. E_g ELECTRONS. DENSITY RANGE FROM 1 TO 2.

Let us consider a situation when the system resonates between one- and two-particle states. It is convenient to introduce a new chemical potential $\mu-U\rightarrow\mu$ and assume that there are no empty states at all.

The four single-particle states $\hat{a}_\sigma^+ |0\rangle$ and $\hat{b}_\sigma^+|0\rangle$ possess spin 1/2. The lowest-energy two-particle states ${}^3A_2$ possess spin $S=1$:

$$\hat{a}_\sigma^+\hat{b}_\sigma^+|0\rangle \quad (S_z=\sigma=\pm 1); \quad \frac{\hat{a}_\uparrow^+\hat{b}_\downarrow^+ + \hat{a}_\downarrow^+\hat{b}_\uparrow^+}{\sqrt{2}}|0\rangle \quad (S_z=0). \tag{2}$$

All higher-energy states ${}^1E$ and ${}^1A_1$ are neglected for simplicity.

A small change in the external magnetic field produces a change in the so-called terminal factors $f_k^{(\sigma)}$ (Ref. 5), each of which equals the sum of the average filling numbers of the initial and final states. Taking account of the symmetry of the system relative to a transposition of the **a** and **b** states, we have

$$f_1^{(\sigma)}=n_{II}^{(\sigma)}+n_I^{(\sigma)}; \quad \delta f_1^{(\sigma)}=\delta n_{II}^{(\sigma)}+\delta n_I^{(\sigma)}; \quad f_2^{(\sigma)}=n_{II}^{(0)}+n_I^{(\overline{\sigma})};$$

$$\delta f_2^{(\sigma)}=\delta n_I^{(\overline{\sigma})}=-\delta n_I^{(\sigma)}. \tag{3}$$

Therefore, in contrast to the ordinary ''one-particle'' case, independent equations are required in order to find the variations of both the one-and two-particle filling numbers. To obtain these equations we shall examine the important part of the expansion of the annihilation operator in terms of the Hubbard $\hat{X}$ operators:

$$\hat{a}_{\mathbf{r}\sigma}=\hat{Z}_{\mathbf{r}}=g_1\hat{X}_{\mathbf{r}}^{(0,\sigma|\sigma,\sigma)}+g_2\hat{X}_{\mathbf{r}}^{(0,\overline{\sigma}|A_0)},$$

where $g_1=1$ and $g_2=1/\sqrt{2}$ are genealogical coefficients. We now multiply this part by an arbitrary linear combination of conjugate $\hat{X}$ operators

$$\hat{Y}_{\mathbf{r}}=\gamma_1\hat{X}_{\mathbf{r}}^{(\sigma,\sigma|0,\sigma)}+\gamma_2\hat{X}_{\mathbf{r}}^{(A_0|0,\overline{\sigma})}.$$

Averaging the separate T products over states with a given temperature and chemical potential in the one-loop approximation, we find a relation between the two-particle filling numbers n_{II}, the Fourier components of the virtual one-particle Green's function $\hat{G}_\omega(\mathbf{p})$, and the terminal factors f_k:

$$g_1\gamma_1 n_{II}^{(\sigma)}+g_2\gamma_2 n_{II}^{(0)}=T\sum_{1\leqslant k,s\leqslant 2}\sum_{\omega\mathbf{p}} g_k G_\omega^{k,s}(\mathbf{p})\gamma_s f_s. \tag{4}$$

The inverse one-particle Green's function matrix is in turn expressed interms of the terminal factors f_k and also in terms of the self-energy matrix $\hat{\Sigma}$, which in the one-loop approximation does not depend on either the frequency or the momentum and in our model is assumed to be reduced to the diagonal form

$$\hat{G}_\omega^{k,s}(\mathbf{p})=[\,\delta_{k,s}(i\omega-\Sigma_s+\mu+\sigma H)-f_k g_k t_{\mathbf{p}} g_s\,]^{-1}. \tag{5}$$

In the zeroth approximation in the external field we obtain two identical terminal factors f_e as well as an equation of state for $1<n_e<2$.

$$K_0=\sum_{\mathbf{p}} n_F(\xi_{\mathbf{p}})=4\frac{n_e-1}{2+n_e}, \quad \xi_{\mathbf{p}}=b_e^2 f_e t_{\mathbf{p}}-\mu; \quad f_e=\frac{2+n_e}{12}. \tag{6}$$

To a first approximation in the applied magnetic field, we find an equation for the susceptibility under the condition $\gamma_k = g_k$:

$$\delta n_{II}^{(\sigma)} = \delta f_2^{(\sigma)} + \delta f_1^{(\sigma)} = \delta R_2 = K_0 \sum_k g_k^2 \delta f_k^{(\sigma)} + f_e D_0 \sum_k g_k^2 \delta\Sigma_k(\sigma)$$

$$+ f_e b_e^2 D_1 \sum_k g_k^2 \delta f_k^{(\sigma)} - f_e b_e^2 D_0 \sigma \delta H, \tag{7}$$

where $g_1^2 = 1$, $g_2^2 = 1/2$, and $b_e^2 = g_1^2 + g_2^2 = 3/2$. We find an equation that is independent of the applied field under the condition $g_1\gamma_1 + g_2\gamma_2 = 0$:

$$\delta n_{II}^{(\sigma)}(1 - K_0) - 2K_0 \delta n_I^{(\sigma)} = \delta f_1^{(\sigma)}(1 - K_0) + \delta f_2^{(\sigma)}(1 + K_0)$$

$$= A(\mu)[\delta\Sigma_1(\sigma) - \delta\Sigma_2(\sigma)], \tag{8}$$

where

$$D_n = \sum_{\mathbf{p}} t_{\mathbf{p}}^n n_F'(\xi_{\mathbf{p}}), \quad A(\mu) = \sum_{\mathbf{p}} \frac{[n_F(\xi_{\mathbf{p}}) - n_F(-\mu)]}{b_e^2 t_{\mathbf{p}}}, \tag{9}$$

and the quantities f_e, $\xi_{\mathbf{p}}$, and K_0 are determined in Eq. (6).

To study the one-loop self-energy diagrams $\Sigma_{1,2}$, it is sufficient to calculate the individual loops and then sum the loops taking account of the commutation rules that determine the nonzero vertex parts of the kinematic interaction.[6,7] In the simplest model with no hybridization we have only the diagonal self-energy parts

$$\Sigma_1^{(a,\sigma)} = -A_2^{(\overline{\sigma})} + B_1^{(\sigma)}; \quad \Sigma_2^{(a,\sigma)} = -A_1^{(\overline{\sigma})} + B_2^{(\overline{\sigma})} + A_2^{(\overline{\sigma})} + B_2^{(\sigma)};$$

$$\Sigma_1^{(b,\sigma)} = -B_2^{(\overline{\sigma})} + A_1^{(\sigma)}; \quad \Sigma_2^{(b,\sigma)} = -B_1^{(\overline{\sigma})} + A_2^{(\overline{\sigma})} + B_2^{(\overline{\sigma})} + A_2^{(\sigma)}; \tag{10}$$

$$A_k^{(\sigma)} = T \sum_{n,\omega,\mathbf{p}} t_{\mathbf{p}}^{k,n} G_\omega^{n,k}(\mathbf{p})$$

is the sum of the products of the matrix elements of the transition matrix $\hat{t}(\mathbf{p})$ by the elements of the virtual Green's function matrix, obtained from the relation (5) and referring to a fixed spin projection and prescribed state a. Note that in a cubic crystal the variation of the self-energy part does not depend on the number of the atomic (a or b) state but changes sign when the spin projection changes sign:

$$\delta\Sigma_1^{(a,\sigma)} = \delta\Sigma_1^{(b,\sigma)} = \delta\Sigma_1(\sigma); \quad \delta\Sigma_2^{(a,\sigma)} = \delta\Sigma_2^{(b,\sigma)} = \delta\Sigma_2(\sigma). \tag{11}$$

We obtain two equations for $\delta\Sigma_k(\sigma)$ from their definition (10) in terms of the integrals of the Green's functions — the so-called one-loop approximation:

$$\delta\Sigma_k^{(\sigma)} = -\delta\Sigma_k^{(-\sigma)} = -[F_{k,n}^{(0)} - D_{k,n}^{(1)}]\delta\Sigma_n^{(\sigma)} + b_e^2 D_{k,n}^{(2)} \delta\phi_n^{(\sigma)} - \sigma \delta H D_1 Q_k. \tag{12}$$

Here the matrices $\hat{D}^{(n)} = D_n \hat{U}$ differ by the temperature factors D_n from Eq. (9) and are proportional to the same matrix $\hat{U}_{n,m} = Q_n g_m^2 / b_e^2$, where $\mathbf{Q} = (3/2, 1/2)$. The operator

$\hat{F}^{(0)}=[K_0-n_F(-\mu)]\hat{V}/f_e b_e^2$ is proportional to the matrix $\hat{V}$, where in the first row the elements $V_{1,1}=V_{1,2}=0$ and the elements in the second row sum to zero: $V_{2,1}=-V_{2,2}=-2/3$.

A consequence of the equations (10)–(12) is a relation that does not depend on either the external field or the terminal factors f_k:

$$g_2^2(\delta\Sigma_1(\sigma)+\delta\Sigma_2(\sigma))=(g_1^2+Q(\mu))(\delta\Sigma_1(\sigma)-\delta\Sigma_2(\sigma)), \tag{13}$$

where $Q(\mu)=[K_0-n_F(-\mu)]/[f_e b_e^2]$. The two relations (3), which relate the variations of the filling numbers and the terminal factors, must be added to this equation. The result is a system of four equations (7), (8), (12) and (13) which are linearized in the external field H. The condition for this equation to be solvable is that the determinant of the following matrix must not vanish:

$$\begin{pmatrix} 1-g_1^2(K_0+f_e b_e^2 D_1) & 1-g_2^2(K_0+f_e b_e^2 D_1) & -f_e D_0 g_1^2 & -f_e D_0 g_2^2 \\ 1-K_0 & 1+K_0 & -A(\mu) & A(\mu) \\ -D_2 b_e^2 g_1^2 & -D_2 b_e^2 g_2^2 & 1-D_1 g_1^2 & -D_1 g_2^2 \\ 0 & 0 & g_2^2-g_1^2-Q & g_1^2+g_2^2+Q \end{pmatrix}. \tag{14}$$

The vanishing of the determinant of this matrix signifies the appearance of ferromagnetic instability.

A calculation of the determinant at $T=0$ gives the equation:

$$K_0(1-K_0)(Q+b_e^2)=-A(\mu)D_2 g_2^2+D_1[f(Q+b_e^2)(g_1^2-g_2^2+b_e^2K_0) + K_0(1-K_0)(Qb_e^2+g_1^4+2g_1^2g_2^2-g_2^4)]. \tag{15}$$

All coefficients depend on the position of the Fermi level. For a semielliptic band model the results can be expressed in terms of the angular parameter α. In the limit $T=0$ we have a unique solution $\alpha_0=2.67$, which corresponds to the existence of a density range $1<n_e<1.26$ where ferromagnetic instability arises.

2. T_{2g} ELECTRONS. DENSITY RANGE FROM 1 TO 2

The results of an analysis of this case are qualitatively the same as in the preceding case. For the semielliptic band model the existence region of the ferromagnetic instability corresponds to the interval $1<n_t<1.4$.

3. T_{2g} ELECTRONS. DENSITY RANGE GREATER THAN 2 BUT LESS THAN 3.

The experimental data indicate that in pure iron (Fe) the electronic states fall between the configurations $3d^24(sp)^6$ and $3d^34(sp)^5$. In this case the saturation magnetic moment equals $2.2\mu_B$. Therefore we shall examine in detail the most interesting case of electronic states resonating between two- and three-particle states.

The lowest three-particle state has spin $S=3/2$ and is four fold degenerate with respect to the spin projection:

$$\hat{a}_\sigma^+\hat{b}_\sigma^+\hat{c}_\sigma^+|\rangle, \quad S_z=3\sigma/2;$$

$$\frac{1}{\sqrt{3}}(\hat{a}_\sigma^+\hat{b}_\sigma^+\hat{c}_{\bar{\sigma}}^+|\rangle+\hat{a}_\sigma^+\hat{b}_{\bar{\sigma}}^+\hat{c}_\sigma^+|\rangle+\hat{a}_{\bar{\sigma}}^+\hat{b}_\sigma^+\hat{c}_\sigma^+|\rangle), \quad S_z=\sigma/2. \tag{16}$$

The X-operator expansion of the transition between three triplet two-particle states of the type (2) and three-particle lowest-energy states (16) is determined by three genealogical coefficients $g_3=1$, $g_4=\sqrt{2/3}$, and $g_5=\sqrt{1/3}$:

$$\hat{a}_{\mathbf{r}\sigma}=\hat{X}_{\mathbf{r}}^{(0,\sigma,\sigma|3\sigma/2)}+\sqrt{\frac{2}{3}}\,\hat{X}_{\mathbf{r}}^{(A(yz,xz)|\sigma/2)}+\frac{1}{\sqrt{3}}\,\hat{X}_{\mathbf{r}}^{(0,\overline{\sigma,\sigma|\sigma/2})}. \tag{17}$$

The equations for the variations of the three-particle filling numbers $\delta n_{III}^{(3\sigma/2)}$ and $\delta n_{III}^{(\sigma/2)}=-\delta n_{III}^{(-\sigma/2)}$ can be obtained from the general equation for the average value of the T products of the annihilation operator (17) by alinear combination of three conjugate operators with arbitrary coefficients γ_s:

$$g_3\gamma_3 n_{III}^{(3\sigma/2)}+g_4\gamma_4 n_{III}^{(\sigma/2)}+g_5\gamma_5 n_{III}^{(-\sigma/2)}=T\sum_{3\leqslant k,n\leqslant 5}\sum_{\omega\mathbf{p}} g_k G_\omega^{k,n}(\mathbf{p})\,\gamma_n f_n. \tag{18}$$

In the one-loop approximation the matrix elements of the one-particle Green's function are determined by the general relation (5).

The terminal factors $f_k^{(\sigma)}$ can be expressed in terms of the filling numbers

$$f_3^{(\sigma)}=n_{III}^{(3\sigma/2)}+n_{II}^{(\sigma)}, \quad f_4^{(\sigma)}=n_{III}^{(\sigma/2)}+n_{II}^{(0)}, \quad f_5^{(\sigma)}=n_{III}^{(-\sigma/2)}+n_{II}^{(-\sigma)}. \tag{19}$$

In a zero field all three terminal factors are identical, $f_k=f_t$, and can be expressed in terms of the electron density n_t, which is related with the chemical potential via the equation of state:

$$f_t=\frac{5n_t-6}{36}; \quad K_0=\sum_{\mathbf{p},} n_F(\xi_{\mathbf{p}})=9\frac{n_t-2}{5n_t-6}. \tag{20}$$

In the case of a finite magnetic field, we employ the obvious relations $\delta n_{III}^{(-\sigma/2)}=-\delta n_{III}^{(\sigma/2)}$, $\delta n_{II}^{(0)}=0$, and $\delta n_{II}^{(-\sigma)}=-\delta n_{II}^{(\sigma)}$. Then we find the relation between the variations of the terminal factors and the filling numbers:

$$\delta n_{III}^{(3\sigma/2)}=\delta f_3^{(\sigma)}+\delta f_4^{(\sigma)}+\delta f_5^{(\sigma)}, \quad \delta n_{III}^{(\sigma/2)}=\delta f_4^{(\sigma)}; \quad \delta n_{II}^{(\sigma)}=-\delta f_4^{(\sigma)}-\delta f_5^{(\sigma)}. \tag{21}$$

The variation of the main equation (18) with $\gamma_k=g_k$ is actually the result of varying the equation of state in a fixed field H:

$$g_3^2\delta n_{III}^{(3\sigma/2)}+b_4^2\delta n_{III}^{(\sigma/2)}+g_5^2\delta n_{III}^{(-\sigma/2)}-K_0\sum_{k=3,4,5} g_k^2\delta f_k^{(\sigma)}-f_t\sum_{k=3,4,5} g_k^2\delta\Sigma_k^{(\sigma)}D_0$$

$$-b_t^2 f\sum_{k=3,4,5} g_k^2\delta f_k^{(\sigma)}D_1=-b_t^2 f_t\sigma\,\delta H D_0. \tag{22}$$

Here we have used the same notation as in Eq. (5) but now $b_t^2=g_3^2+g_4^2+g_5^2=2$.

If the vector γ is directed perpendicular to the vector **g**, i.e., $\Sigma_{3\leqslant k\leqslant 5}\gamma_k g_k=0$, then two relations can be obtained which do not depend explicitly on the magnetic field. We find the first equation under the conditions $g_5\gamma_5=g_3\gamma_3$ and $g_4\gamma_4=-2g_3\gamma_3$.

$$(1-K_0)(\delta n_{III}^{(3\sigma/2)}-3\,\delta n_{III}^{(\sigma/2)})-A(\mu)(\delta\Sigma_3(\sigma)-2\,\delta\Sigma_4(\sigma)+\delta\Sigma_5(\sigma))=0. \tag{23}$$

Setting $\gamma_4=0$ and $g_5\gamma_5=-g_3\gamma_3$, we obtain the second equation:

$$(1-K_0)(\delta n_{III}^{(3\sigma/2)}+\delta n_{III}^{(\sigma/2)})-2K_0\,\delta n_{II}^{(\sigma)}-A(\mu)(\delta\Sigma_3(\sigma)-\delta\Sigma_5(\sigma))=0. \tag{24}$$

Here the coefficient K_0 is determined by the equation of state (20) and the coefficient $A(\mu)$ is determined by a relation of the type (9) but with the substitutions $b_e^2\to b_t^2$ and $f_e\to f_f$.

It is evident that in the absence of a field all self-energy parts are equal and give a small correction to the chemical potential.

Our next problem is to calculate the corrections $\delta\Sigma_k$ which are proportional to the first power of the magnetic field. We obtain three equations for $\delta\Sigma_k$ from their definitions (25) in terms of integrals of the product of the Green's function (7) by the hopping integral $t_{\mathbf{p}}$:

$$\delta\Sigma_k^{(\sigma)}=-\delta\Sigma_k^{(-\sigma)}=-[F_{k,n}^{(0)}-D_{k,n}^{(1)}]\delta\Sigma_n^{(\sigma)}+b_t^2D_{k,n}^{(2)}\delta f_n^{(\sigma)}-\sigma\delta HR_kD_1, \tag{25}$$

$$\hat{D}^{(n)}=\sum_{\mathbf{p}}\,t_{\mathbf{p}}^n n_F'(\xi_{\mathbf{p}})\hat{U}.$$

Here the operators differ by the temperature factor and are proportional to the same matrix $\hat{U}_{k,m}=R_kg_m^2/b_t^2$, where $\mathbf{R}=(7/3,1,-1/3)$. The operator $\hat{F}^{(0)}=Q(\mu)\hat{W}$, where $Q(\mu)=[K_0-n_F(-\mu)]/f_tb_t^2$. The elements of each row in the matrix $\hat{W}$ sum to zero:

$$\hat{W}=\begin{pmatrix} U_{3,3}-2g_3^2=-\frac{5}{6}; & U_{3,4}=\frac{7}{9}; & U_{3,5}-g_5^2=\frac{1}{18} \\ U_{4,3}=\frac{1}{2}; & U_{4,4}-3g_4^2=-\frac{5}{3}; & U_{4,5}+3g_5^2=\frac{7}{6} \\ U_{5,3}-b_3^2=-\frac{7}{6}; & U_{5,4}+3g_4^2=\frac{17}{9}; & U_{5,5}-2g_5^2=-\frac{13}{18} \end{pmatrix}. \tag{26}$$

Ferromagnetic instability is due to the appearance of an infinite magnetic susceptibility. This condition is equivalent to the possibility of solving a system of six homogeneous equations corresponding to Eqs. (15), (16), (18), and (25). The direct calculation of the sixth-order determinant gives the equation:

$$[3K_0(1-K_0)-2f_tD_1(2+3K_0)][18+52Q+9Q^2-D_1(26+68Q-35Q^2)]$$
$$=2D_2[f_tD_0(2+3K_0)(14+40Q-11Q^2)-2A(\mu)(14+40Q+9Q^2)]. \tag{27}$$

A calculation of the coefficients in Eq. (27) for the semielliptic band model and at $T=0$ shows that ferromagnetic instability exists in a quite narrow density interval: $2<n_t<2.16$.

4. CONCLUSIONS

The main result of this letter is the discovery of magnetic ordering when with a small number of excitations for each cell the ground state is a high-spin, disordered state and is determined according to Hund's rule. This result corresponds qualitatively to ferromagnetism in cobalt and α-iron, which possess a nonintegral number of unpaired spins $n_e = 1.6$ and $n_t = 2.2$, respectively.

[1] J. Hubbard, Proc. R. Soc. A **296**, 82, 100 (1967).
[2] J. Goodenough, Phys. Rev. **120**, 67 (1960).
[3] E. C. Stoner, Phil. Mag. **22**, 81 (1936).
[4] J. Hubbard and K. P. Jain, J. Phys. C **2**, 1650 (1968).
[5] R. O. Zaĭtsev, Zh. Éksp. Teor. Fiz. **70**, 1100 (1976) [Sov. Phys. JETP **43**, 574 (1976)].
[6] F. Dyson, Phys. Rev. **102**, 1217, 1230 (1956).
[7] R. O. Zaĭtsev, Phys. Lett. A **134**, 199 (1988).

Translated by M. E. Alferieff

Instability of the two-dimensional metallic phase to a parallel magnetic field

V. M. Pudalov[a)]
Institut für Halbleiterphysik, Johannes Kepler Universität Linz, A-4040 Linz, Austria; Institute for High Pressure Physics, 142092 Troitsk, Moscow Region, Russia

G. Brunthaler, A. Prinz, and G. Bauer
Institut für Halbleiterphysik, Johannes Kepler Universität Linz, A-4040 Linz, Austria

(Submitted 20 May, 1997)
Pis'ma Zh. Éksp. Teor. Fiz. **65**, No. 12, 887–892 (25 June 1997)

Magnetotransport studies of the unusual two-dimensional metallic phase in high-mobility Si–MOS structures are reported. It is found that a magnetic field applied in the 2D plane suppresses the metallic state, causing the resistivity to increase dramatically (by more than 30 times). The total existence range of the metallic state is found to contain three distinct types of magnetoresistance, related to the corresponding quantum corrections to the conductivity. The data suggest that the unusual metallic state is a consequence of both spin and Coulomb interaction effects. © *1997 American Institute of Physics.*
[S0021-3640(97)00712-3]

PACS numbers: 73.40.Hm, 71.30.+h

Recently, convincing evidence for the existence of a 2D metallic state in Si–MOS structures at zero magnetic field has been obtained in studies of the quantum Hall effect at insulator transitions[1] and of the Global Phase Diagram.[2] The extended states, which in high magnetic field H are centered in the corresponding Landau bands, were found experimentally to merge and remain in a finite energy range as H approaches 0, thus providing direct transitions from the high-order quantum Hall effect states to the insulator.[1] This behavior could not be expected in the framework of the one-parameter scaling theory (OPST),[3] where the extended states are anticipated to ''float up'' in energy as $H \rightarrow 0$ (Ref. 4). The experimental findings thus prove the existence of a mobility edge, whereas the predicted floating would evidently correspond to complete localization. In subsequent direct studies[5,6] the conductivity in high-mobility Si–MOS structures in zero magnetic field was found to scale with temperature and electric field, and the scaling parameter exhibited a pronounced critical behavior appropriate for a metal–insulator transition.

The observations of the metal–insulator transition at zero magnetic field in two dimensional system raised two major questions: (i) what is the origin of this unforeseen transition, and (ii) whether or not the one-parameter scaling theory[3] is correct in predicting the absence of the metallic state in two dimensions. The majority of experimental data on 2D systems in fact support the results of calculations of the ''quantum corrections'' to the classical diffusion[7–9] rather than the scaling theory in total.

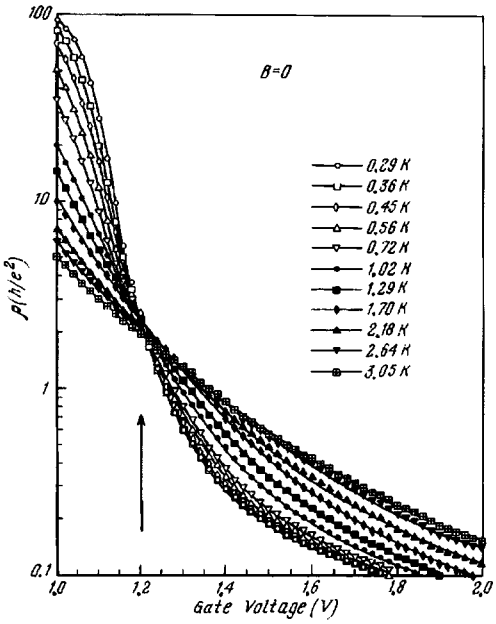

FIG. 1. Resistivity versus gate voltage measured on sample Si-22. Different symbols correspond to 11 temperature values. The electron density is related to the gate voltage by $n=1.205\times10^{11}(V_g-0.4)$, where n is in cm^{-2} and V_g in volts.

Recently a strong influence of the in-plane magnetic field on the resistivity has been found in Si/SiGe super lattices[10] as well as in high-mobility Si–MOS structures.[11] In the current work we report some new experimental evidence for the origin of the metal–insulator transition in Si structures and test the applicability of the weak localization corrections. We have observed that the magnetic field applied in the 2D plane destroys the metallic state and restores the weakly or strongly localized regimes. Over the existence range of the metallic state we have found *three distinct types* of magnetoresistance, related to the corresponding quantum corrections due to interference and interactions.[7,8]

The magnetotransport measurements were performed by a 4-terminal dc technique. Four Si–MOS structures were studied: Si-15A with peak mobility (at 0.3 K) $\mu=41{,}000$ $\mathrm{cm}^2/\mathrm{V}\cdot\mathrm{s}$, Si-2Ni with $\mu=38{,}000$, Si-22 with $\mu=26{,}000$, and Si-39 with $\mu=5{,}000$. While the first three samples exhibited the metal–insulator transition[5,6] and a sharp drop in resistance at $T<2-3$ K, the latter low-mobility sample does not show a substantial decrease in resistance.

Figure 1 shows a set of resistivity curves at different temperatures, typical for high-mobility samples.[5] At carrier density higher than the critical density n_c (indicated by an arrow) the resistance *increases* with temperature, while at lower densities it *decreases*. The intercept is slightly dependent on temperature. The corresponding separatrix between the metallic and insulating sets of $\rho(T)$ curves in Fig. 2 is rising as T decreases.

Figure 2a represents the ''metallic'' (or high-density) part of the $\rho(T,n_s)$ plot and

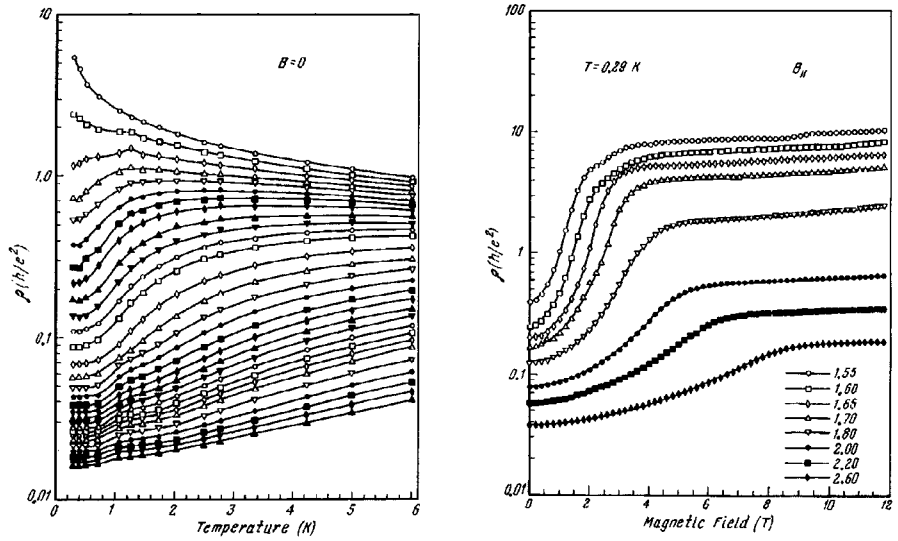

FIG. 2. Resistivity versus temperature for the metallic range of densities, measured on sample Si-15A at zero field. Different curves correspond to electron densities between 0.83 and 3.72×10^{11} cm^{-2}. (b) Resistivity versus parallel magnetic field, measured at $T=0.29$ K on sample Si-15 A. Different symbols correspond to gate voltages from 1.55 to 2.6 V, or, equivalently, to densities from 1.01 to 2.17×10^{11} cm^{-2}.

shows a strong drop (by $5\times$) in the resistivity below $\sim$2 K. As T approaches 0,$\rho(T)$ saturates and does not show a tendency to increase, at least down to 14 mK. The lowest mobility sample Si-39 does not display a decrease in ρ apart from a few percent in the range 4 to 0.02 K; the latter behavior agrees completely with the OPST.

EFFECT OF THE MAGNETIC FIELD PARALLEL TO THE 2D PLANE

The application of an in-plane magnetic field results in a dramatic increase of the resistance, more than 2 orders of magnitude, as seen in Fig. 2b. At high fields, the resistance saturates. This behavior was found in all three high-mobility samples, in agreement with the results of Ref. 11.

At high electron densities, the saturation level $\rho^*(H=12.5\text{ T}, T\to0)$ seems similar to the saturation level at high temperatures and zero field, $\rho^*(H=0,T=6\text{ K})$, i.e., to the resistivity anticipated in the OPST-like behavior. Thus, the magnetic field simply destroys the metallic state. Comparison of the two plots (Figs. 2a and 2b) reveals a remarkable similarity between the effects of temperature and magnetic field on the resistivity at high densities. Both factors destroy the metallic state and restore the weakly or strongly localized regimes. At densities lower than 2×10^{11} and closer to the critical density n_c, a magnetic field also gives rise to an additional ten times larger positive magnetoresistance.

It has been noticed earlier[12] that the temperature dependence of the resistivity of the 2D metallic phase may be well described by an empirical law $\rho(T)=\rho_1+\rho_2\exp(-T^*/T)$, where ρ_1 is due to scattering at $T=0$, while the second term

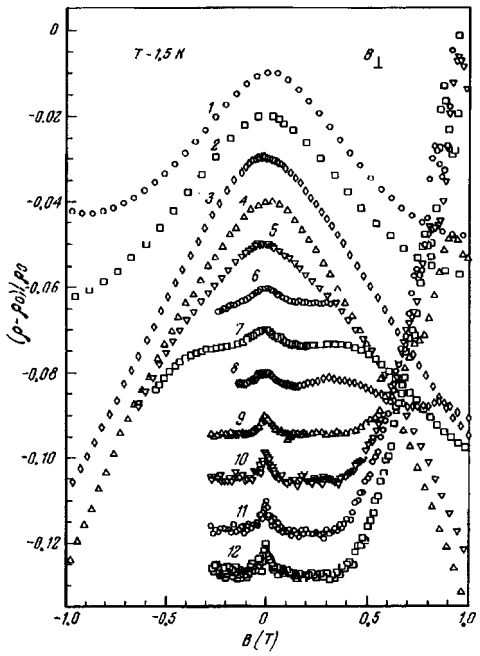

FIG. 3. Normalized magnetoresistance $(\rho(H)-\rho(0))/\rho(0)$ versus the perpendicular magnetic field for different densities on sample Si-2Ni at $T=1.48$ K. The curves labeled *1* to *12* correspond to the density values of 0.90, 0.96, 1.12, 1.34, 1.56, 2.01, 2.12, 2.67, 3.77, 4.88, 5.98, and 7.09×10^{11} cm^{-2}. The curves have been shifted relative to each other vertically by 0.01.

is associated with an energy gap, $\Delta=kT^*$. Since a parallel field does not affect orbital electron motion, the magnetic field may couple to the 2D electrons only via their spins. Our results therefore point to a spin-related origin of the unusual metallic state and of the energy gap Δ.

WEAK LOCALIZATION CORRECTIONS

In a weak perpendicular magnetic field, $H<0.1$ T, all three high-mobility samples exhibited weak magnetoresistance, similar to the earlier reported data Ref. 12. The narrow peak in $\rho(H)$ seen in Fig. 3 is sensitive to the normal component of the field and is missing when the field is aligned with the 2D plane within ±7 min. Its amplitude does not vary much with density in the range $(9-100)\times10^{10}$cm^{-2}. These features allow us to attribute the narrow peak to the orbital single-particle quantum interference correction. At higher fields, $H>0.2$ T, and at high density, $n>4\times10^{11}$ cm^{-2}, the positive parabolic magneto resistance dominates in both the parallel and perpendicular field orientation. This indicates a spin-related origin of the positive magnetoresistance component. In a perpendicular field the negative magnetoresistance with decreasing density, overcomes the positive magnetoresistance, and eventually becomes so large that it prevents the observation of the quantum interference peak. The negative magnetoresistance persists to

the insulating range of densities, where it has been explained in terms of a field effect on the tunneling conductance.[14] The negative magnetoresistance is not seen in a parallel field and is therefore related to the orbital electron motion.

The positive parabolic magnetoresistance is usually considered as a quantum correction due to the interaction associated with the Zeeman splitting, while the negative magneto resistance is associated with a correction due to electron–electron correlations.[7,8] The transition from the spin-dominated to the Coulomb-dominated interaction occurs at a density $n^* \approx 2.8 \times 10^{11}$ for Si-15A and Si-2Ni, and $n^* = 1.7 \times 10^{11}$ for Si-22. These values are noticeably higher than the critical density at the mobility edge, which is $n_c = 9.0 \times 10^{10}$ for Si-15A and Si-2Ni and at $n_c = 10.2 \times 10^{10}$ for Si-22. Therefore, the spin effects and, partly, the Coulomb effects govern the resistivity over the existence range of the metallic phase.

The persistence of the quantum corrections to the conductivity over the total range of existence of the metallic state (see Fig. 3) seems to justify the applicability of the quantum corrections approach to the unusual 2D metal. On the quantitative side, if we attribute the positive magnetoresistance (shown in Fig. 2b) to the Zeeman interaction term in the quantum corrections, than we come up with the conclusion that the interaction-related quantum corrections are ''blowing up'' in the vicinity of the metal–insulator transition, giving rise to an enhancement factor of up to about 10^2 to the $\Delta\rho(H)/\rho$ values. This is not surprising, since the relevant theoretical calculations were done in the limit $k_F l \gg 1$, where thecorrections are small, whereas in the vicinity of the metal–insulator transition, at $k_F l \sim 1$, the quantum corrections may become large.

DISCUSSION

Considering the possible features in which the high-mobility Si–MOS structures differ from other systems, like GaAs/Al(Ga)As where the mobility edge was not found Ref. 15, we would like to note the following: (i) the Coulomb interaction energy $E_{ee} = e^2/\kappa r$ is higher in Si–MOS structures than in GaAs samples (at the same interelectron distance, r) by a factor of 1.7 due to the smaller dielectric constant $\kappa = 7.7$ at the Si/SiO_2 interface,[1] (ii) the Si/SiO_2 interface is characterized by a very strong asymmetry of the confining potential in the z direction. The latter results in a large effective Lorenzian field H^* seen by electrons; the corresponding spin–orbit gap at zero field was found to be equal to ≈ 4 K (Ref. 12). These effects associated with the broken reflection symmetry of the confining potential are much less pronounced in GaAs/Al(Ga)As heterojunctions and are apparently absent in rectangular potential wells.

It is known that the inclusion of the spin changes the universality class of a 2D system. The corresponding scaling arguments are is based only on the symmetry arguments and should not depend much on the particular microscopic mechanism. The above spin-related mechanism may be important if the relevant energy gap $\Delta = g\mu H^*$ is larger than the spin-level broadening $\Gamma = h/\tau$. It appears that the Δ/Γ ratio is ≈ 3 for Si-15A and Si-2Ni, while $\Delta/\Gamma \approx 1$ for the low-mobility sample Si-39, which exhibits normal scaling behavior and no metal–insulator transition.

Thus, based on the data presented here we suggest that the metallic state and metal–insulator transition in high-mobility Si–MOS structures may be a consequence of both

the spin and the Coulomb interaction effects. The former are enhanced by the broken reflection symmetry of the confining potential well, while the latter provide the necessary large relaxation time in the low electron-density range.

Recently some alternative suggestions on the origin of the unusual 2D metallic state in Si–MOS structures have been made, namely, that it may be induced by the Coulomb interaction,[16] or by spin-triplet pairing,[17] or that it might be a manifestation of non-Fermi-liquid behavior.[18]

One of the authors (V. M. P.) benefited from fruitful discussions with D. Khmelnitskii, V. Kravtzov and I. Suslov. The authors acknowledge support by the Russian Fund for Fundamental Research (Grant 97-02-17387), by the Russian State Committee for Science and Technology (in the framework of the Programs ''Physics of Solid-State Nanostructures'' and ''Statistical Physics''), by NWO of The Netherlands, and by FWF of Austria.

[a)]e-mail:pudalov@ns.hppi.troitsk.ru

---

[1] V. M. Pudalov, M. D'Iorio, and J. W. Campbell, JETP Lett. **57**, 608 (1993); V. M. Pudalov, M. D'Iorio, and J. W. Campbell, Surf. Sci. **305**, 107 (1994).
[2] S. V. Kravchenko, W. Mason, J. E. Furneaux, and V. M. Pudalov, Phys. Rev. Lett. **75**, 910 (1995).
[3] E. Abrahams, P. W. Anderson, D. C. Licciardello, and T. V. Ramakrishnan, Phys. Rev. Lett. **42**, 673 (1979).
[4] D. E. Khmelnitskii, Phys. Lett. **106**, 182 (1984).
[5] S. V. Kravchenko, J. E. Furneaux, M. D'Iorio, and V. M. Pudalov, Phys. Rev. B **49**, 8039 (1994).
[6] S. V. Kravchenko, W. E. Mason, G. E. Bowker *et al.*, Phys. Rev. B **51**, 7038 (1995); S. V. Kravchenko, D. Simonian, M. P. Sarachik *et al.*, Phys. Rev. Lett. **77**, 4938 (1996).
[7] G. Brunthaler, T. Dietl, M. Sawicki *et al.*, Semicond. Sci. Technol. **11**, 1624 (1996).
[8] D. Simonian, S. V. Kravchenko, and M. P. Sarachik, cond-mat/9704071.
[9] B. L. Altshuler and A. G. Aronov, in *Electron–Electron Interaction in Disordered Systems*, ed. by A. L. Efros and M. Pollak, Amsterdam: North-Holland, 1985.
[10] H. Fukuyama, *ibid.*, p.155.
[11] V. M. Pudalov, *op. cit.* 18, p. 34.
[12] D. J. Bishop, R. J. Dynes, and D. C. Tsui, Phys. Rev. B **26**, 773 (1982).
[13] A. E. Voiskovsky and V. M. Pudalov, JETP Lett. **62**, 947 (1995).
[14] A. J. Dahm, F. W. Van Keuls, H. Mathur, and H. W. Jiang, *op. cit.* 18, p. 33.
[15] A. Efros, F. G. Pikus, and E. V. Tsiper, *op. cit.* 16, p. 10.
[16] For recent results see: *Proceedings of the International Conference on Electron Localization and Quantum Transport in Solids*, Jaszowiec, Poland, 1996, ed. by T. Dietl, Inst. of Physics PAN, Warsaw, 1996.
[17] D. Belitz, and T. R. Kirkpatrick, cond-mat/9705025.
[18] V. Dobrosavljevic, E. Abrahams, E. Miranda, and S. Chakravarty, cond-mat/9704091.

Published in English in the original Russian journal. Edited by Steve Torstveit.

Characteristic features of the temperature dependence of the surface impedance of $YBa_2Cu_3O_{6.95}$ single crystals

M. R. Trunin,[a)] A. A. Zhukov, G. A. Emel'chenko, and I. G. Naumenko
Institute of Solid-State Physics, Russian Academy of Sciences, 142432 Chernogolovka, Moscow District, Russia

(Submitted 22 May 1997)
Pis'ma Zh. Éksp. Teor. Fiz. **65**, No. 12, 893–898 (25 June 1997)

The real and imaginary parts of the surface impedance $Z_s=R_s+iX_s$ of $YBa_2Cu_3O_{6.95}$ single crystals are measured at a frequency $\omega/2\pi=9.4$ GHz. The quantities $R_s(T)$ and $X_s(T)$ are linear functions of temperature for $T<0.3T_c$ ($T_c=93.5$ K). A maximum of $R_s(T)$ and a plateau of $X_s(T)$ are observed in the interval $35<T<65$ K. Our experimental data, just as all recent measurements of $R_s(T)$ in $YBa_2Cu_3O_{6.95}$ single crystals in the temperature range $0<T<1.3T_c$, are described well in a two-fluid model which assumes electron–phonon scattering of quasiparticles. © *1997 American Institute of Physics.* [S0021-3640(97)00812-8]

PACS numbers: 74.25.Nf, 74.72.Bk

The linear temperature dependences of the surface resistance $R_s(T)$ and reactance $X_s(T)$ in the range $T<T_c/3$ which were observed in microwave measurements of the impedance $Z_s=R_s+iX_s$ of $YBa_2Cu_3O_{6.95}$(YBCO) single crystals[1] provoked a wide discussion of the symmetry of the order parameter in high-T_c superconductors. In the microscopic models, the linear low-temperature variation of the penetration depth $\lambda(T)=X_s(T)/\omega\mu_0$ of the field is due to the fact that the order parameter vanishes at the Fermi surface. According to the theory, the dependence $\lambda(T)\propto T$ holds: a) in the case of $d_{x^2-y^2}$ symmetry of the order parameter,[2] b) for anisotropic s-type symmetry,[3] when scattering by magnetic impurities leads to gapless superconductivity, and c) in models with mixed $d+s$ symmetry.[4] The quasiparticle relaxation mechanism is especially important in calculations of the real part $R_s(T)$ of the impedance. For inelastic scattering by antiferromagnetic spin fluctuations in the case a) (Ref. 5) and for the electron–phonon interaction in the case b) (Ref. 6) the computed curves $R_s(T)$ had a wide maximum in the region $T\sim T_c/2$; such a maximum has been observed in high-quality YBCO single crystals. However, a linear temperature dependence of $R_s(T)$ at low temperatures was not obtained in microscopic models. In measurements of the impedance of $Bi_2Sr_2CaCu_2O_8$ (Ref. 7) and $Ba_{0.6}K_{0.4}BiO_3$ (Ref. 8) single crystals at frequency $\sim$10 GHz, a linear variation of the surface resistance was observed in an even wider temperature interval $0<T\leqslant T_c/2$. A phenomenological model describing all above-indicated low-temperature features of the curves $Z_s(T)$ in single crystals of high-T_c superconductors was proposed in Ref. 8.

Recent experiments[9–11] with YBCO samples have demonstrated that the contribu-

tion of the CuO_2 planes and CuO chains to the measured quantities must be taken into account simultaneously. This imposes definite restrictions on the symmetry of the order parameter in YBCO. New features of $Z_s(T)$, which do not agree with the purely $d_{x^2-y^2}$-wave picture of superconducting pairing, have been found in the microwave response of single crystals[9] at intermediate temperatures and at temperatures close to T_c.

In the present work we measured the temperature dependences of the surface impedance of YBCO single crystals. These dependences also demonstrate differences from existing results[1] in the intermediate temperature range. In the two-fluid model all temperature dependences $R_s(T)$ which we observed also in Refs. 1 and 9 are described well assuming an electron–phonon quasiparticle-scattering mechanism. Taking account of the features of the behavior of $\lambda(T)$, which are common to all experiments, at low and close to T_c temperatures, we have found an equation describing the curves $\lambda^2(0)/\lambda^2(T)$ in the entire temperature interval.

The YBCO single crystals were grown using the standard yttrium-stabilized zirconium dioxide crucibles. The melt contained 12–15 mole % YBCO and 88–85% of the eutectic mixture 28% BaO:72% CuO. The initial components Y_2O_3, BaO_2, and CuO were 99.95, 99.90, and 99.95% pure, respectively. Our sample preparation method differed from the methods employed in Ref. 12 (ZrO_2 crucibles) and Ref. 13 ($BaZrO_3$ crucibles) mainly in that the homogenization time of the growth solution and the crystal growth time were much shorter. The homogenization time of the fluxed melt at $T=1000$ °C did not exceed 1 h because of the fact that accelerated–decelerated rotation of the crucible was used,[14] which made intense mixing of the melt possible. The single crystals were grown by the temperature-differential method in a time of 2–3 min under conditions of morphological stability of the crystallization front. The crucible was decanted at $T=955$ °C and cooled down to room temperature at a rate of 30 °C/h. The single crystals were saturated with oxygen at $T=500$ °C in an oxygen flow, after which their critical temperature was equal to 92–94 K. The measurements of the dynamic susceptibility showed that the width of the superconducting transition in the samples did not exceed 0.2 K.

The surface impedance of single crystals with the characteristic dimensions $1.5\times1.5\times0.1$ mm was measured at a frequency of 9.43 GHz. A sample at the end of a sapphire rod was placed at the center of a superconducting niobium cavity operating on the H_{011} mode. A microwave magnetic field, oriented parallel to the $\hat{c}$ axis of the crystal, produces circulation of the high-frequency currents in the ab plane. The numerical values of the surface resistance $R_s(T)$ and reactance $X_s(T)$ were determined by the standard procedure[1,15] from the values of Q and the shift of the resonance frequency measured as functions of the temperature.

Figure 1 displays the typical curves of $R_s(T)$ and $X_s(T)$ in the temperature interval $4.2\leqslant T\leqslant 125$ K. In accordance with the condition of the normal skin effect $R_s(T)=X_s(T)$ for $T\geqslant T_c=93.5$ K. From the experimental value $R_s(T_c)=\sqrt{\omega\mu_0\rho(T_c)/2}\simeq 0.12\ \Omega$ we find the resistivity $\rho(T_c)\simeq 38\ \mu\Omega\cdot$cm.

The low-temperature behavior of $R_s(T)$ and $\lambda(T)=X_s(T)/\omega\mu_0$ is demonstrated in Fig. 2. Both dependences are linear in the temperature range $T<30$ K. Continuing the $R_s(T)$ line to $T=0$, we obtain the residual surface resistance $R_s(0\ \text{K})\equiv R_{\text{res}}\simeq 235\ \mu\Omega$.

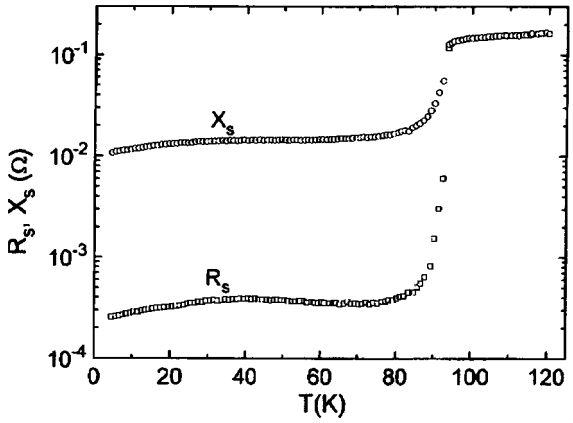

FIG. 1. Temperature dependences of the surface resistance R_s and reactance X_s in a YBCO single crystal.

Similarly, we find the well-known value $\lambda(0) \simeq 1400$ Å for the ab plane in YBCO. The maximum of $R_s(T)$ characteristic for perfect YBCO crystals is observed near $T \simeq 40$ K. In contrast to Ref. 1, we also see a plateau in the curves $\lambda(T)$ or $X_s(T)$ in the interval $35 < T < 65$ K. Something similar has been observed in microwave experiments with high-quality epitaxial films[16] and YBCO single crystals,[9] where a bump appears near 60 K against the background of a monotonic temperature dependence $\lambda(T)$.

We shall attempt to describe the results of our measurements in terms of a two-fluid model, according to which the real σ_1 and imaginary σ_2 parts of the complex conductivity σ_s of a high-T_c superconductor at microwave frequencies ($\omega\tau \ll 1$) are

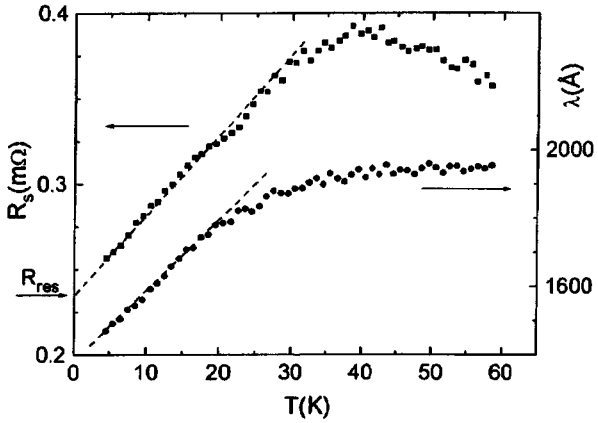

FIG. 2. Low-temperature dependences of R_s and the penetration depth $\lambda = X_s/\omega\mu_0$ of the field. The dashed straight-line segments were drawn by eye. The value $R_s(0\ \text{K}) \equiv R_{\text{res}}$ is indicated.

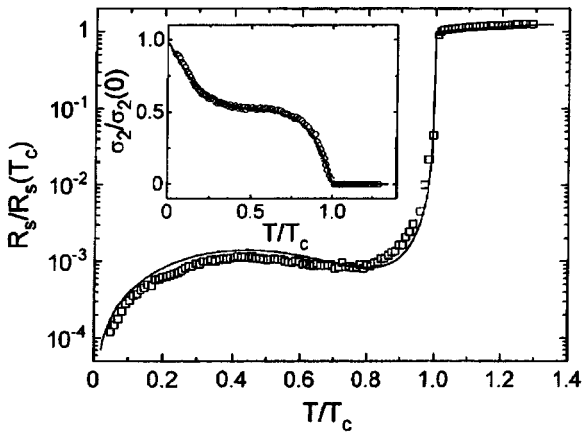

FIG. 3. Comparison of the computed (curves), from Eqs. (1)–(3) and (5), and experimental (dots) temperature dependences of the surface resistance $R_s(t)/R_s(T_c)$ and the imaginary component of the conductivity $\sigma_2(t)/\sigma_2(0)$ (inset). The temperature-dependent part $R_s(T)$ was obtained from the measured value of R_s in Figs. 1 and 2 by subtracting the residual surface resistance $R_{\rm res}$.

$$\sigma_s \equiv \sigma_1 - i\sigma_2, \quad \sigma_1 = \frac{e^2\tau}{m} n_n, \quad \sigma_2 = \frac{e^2}{m\omega} n_s, \tag{1}$$

where n_s is the density of superconducting carriers and n_n is the density of normal carriers, both types of carriers having the same charge e and mass m; τ is the relaxation time. The total carrier density n at any temperature $t \equiv T/T_c \leqslant 1$ equals the sum $n_n(t) + n_s(t)$. The conductivity $\sigma_s(t)$ is related with the surface impedance by the local relation

$$Z_s(t) = R_s(t) + iX_s(t) = \sqrt{i\omega\mu_0/\sigma_s(t)}. \tag{2}$$

The measured temperature dependence $\lambda^2(0)/\lambda^2(t) = \sigma_2(t)/\sigma_2(0) = n_s(t)/n$ is shown (circles) in the inset in Fig. 3. Given the values of $n_s(t)/n$ and therefore $n_n(t)/n = 1 - n_s(t)/n$ the function $\tau(t)$ is the only remaining function of temperature left to determine in order to determine the conductivity $\sigma_s(t)$ in Eq. (1) and the impedance $Z_s(t)$ in Eq. (2). To describe the experimental dependences $R_s(T)$ we employ the expression

$$\frac{1}{\tau(t)} = \frac{1}{\tau(T_c)} \frac{\beta + t^5}{1 + \beta}, \tag{3}$$

where $\beta \approx \tau(T_c)/\tau(0) \ll 1$ is a numerical parameter.[8] The expression (3) corresponds to the low-temperature limit of the Bloch–Grüneisen formula, which can be put into the form

$$\frac{1}{\tau(t)} = \frac{1}{\tau(T_c)} \frac{\beta + t^5 \mathcal{J}_5(\kappa/t)/\mathcal{J}_5(\kappa)}{1 + \beta}, \quad \mathcal{J}_5(\kappa/t) = \int_0^{\kappa/t} \frac{z^5 e^z dz}{(e^z - 1)^2}, \tag{4}$$

where $\kappa=\Theta/T_c$ and Θ is the Debye temperature. For $\kappa\gg 1$ the relation (3) follows from Eq. (4).

Setting $\beta=0.2$ in Eq. (3) and taking the experimental values $n_s(t)/n=\sigma_2(t)/\sigma_2(0)$ and $\omega\tau(T_c)=(\rho(T_c)\sigma_2(0))^{-1}=0.004$, we find from Eqs. (1) and (2) the dependence $R_s(t)/R_s(T_c)$ shown by the curve in Fig. 3; this curve is virtually matches the measured quantities (squares) in the entire temperature interval. Hence we conclude that the electron–phonon scattering mechanism plays the determining role in forming the signal $R_s(T)$.

We shall now try to describe the dependence $\sigma_2(t)/\sigma_2(0)$ itself. We note that the linear section of this dependence at low temperatures and the steep slope of the curves in Fig. 3 near T_c are characteristic of all measurements of the impedance of high-quality YBCO single crystals. The linear low-temperature variation of $\lambda(T)$ and $R_s(T)$ in the model of Ref. 8 was described well by the function $n_s(t)\propto(1-t)^{\alpha}$, where α is a numerical parameter. In the inset in Fig. 3 the derivative$(1/\sigma_2(0))d\sigma_2(t)/dt=(1/n)dn_s(t)/dt$ at $t=1$ equals -4. This value is identical to that obtained from the two-fluid Gorter–Casimir model $(n_s(t)\propto(1-t^4))$ and, as shown in a number works,[17] corresponds to an average electron–phonon interaction greater than 1. For arbitrary temperature $T\leqslant T_c$ we write a general expression that corresponds to the indicated behavior of $n_s(t)$ in both limits — low and close to T_c temperatures,

$$n_s/n=(1-t)^{\alpha}(1-\delta)+\delta(1-t^{4/\delta}), \tag{5}$$

where $0<\delta<1$ is a weighting factor. The line representing the function (5) with $\alpha=5.5$ and $\delta=0.5$ agrees very well with the experimental values of $\sigma_2(t)/\sigma_2(0)$.

So, all observed features of the temperature dependence of the impedance of YBCO are described in the proposed two-fluid model. The equations (1)–(5) also describe our measurements of $Z_s(T)$ for other YBCO single crystals grown by a similar method. Furthermore, we checked the applicability of the model for describing the experimental results of Refs. 1 and 9 obtained by other authors.

Figure 4 displays the data taken from Ref. 9. The circles correspond to the measurements performed in Ref. 1 on YBCO single crystals grown using ZrO_2 crucibles (YSZ).[12] The only difference from the measurements in Ref. 1 are that the values of $R_s(T)$ are too low in the liquid-nitrogen temperature range: The value of $R_s(77\ \mathrm{K})$ observed in Ref. 1 was always higher than $R_s(4.2\ \mathrm{K})$. The measured value $\omega\tau(T_c)=0.003$. The dashed curves show the computational results obtained with Eqs. (1)–(3) and (5) and agree well with the experimental values when $\alpha=0.8$, $\beta=0.01$, and $\delta=0.3$.

The squares in Fig. 4 correspond to the new results[9] obtained for YBCO crystals from $BaZrO_3$ crucibles (BZO).[13] Two distinguishing features are seen: a relatively small temperature interval $0<T\ll T_c$ of a linear variation of $\sigma_2(t)$, which rapidly converts into a quadratic variation with increasing temperature, and an appreciable rise of $R_s(t)/R_s(T_c)$ for $t>0.5$, increasing rapidly very close to T_c. Nonetheless, taking the experimental values of $\sigma_2(t)/\sigma_2(0)$ and $\omega\tau(T_c)=0.004$ and using for $1/\tau(t)$ expression (4) with $\beta=0.02$ and $\kappa=4$, we obtain from Eqs. (1) and (2) the temperature dependence $R_s(t)/R_s(T_c)$ shown by the solid curve in Fig. 4 and demonstrating all experimental features (squares). This confirms once again the conclusion that quasiparticles in YBCO

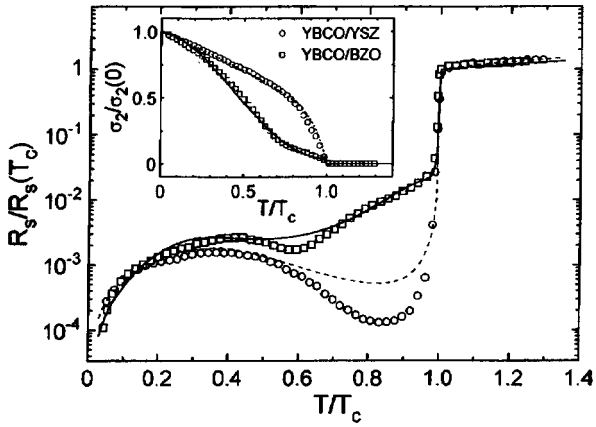

FIG. 4. Circles — experimental data for YBCO (YSZ) single crystals; squares — data for YBCO (BZO) taken from Ref. 9. The dashed and solid lines were computed using Eqs. (1)–(5) of the model.

relax by the electron–phonon mechanism. The transition from the linear to the quadratic regime in $\sigma_2(t)$ for $t \ll 1$ can be described by introducing an additional factor $(1+\eta t)$ in the first term for $n_s(t)$ in Eq. (5). Then the solid line in the inset in Fig. 4 obtains for $\alpha = 2.2$, $\eta = 2$, and $\delta = 0.04$.

Therefore all features of the measured temperature dependences $Z_s(T)$ for YBCO single crystals are described in the two-fluid model considered above, despite the difference in the measured temperature dependences $Z_s(T)$ in YBCO single crystals prepared by different methods.

This letter has examined the characteristic features in the temperature dependence of the surface impedance of high-quality YBCO single crystals.Our measured curves (Fig. 3) fall between the existing[1] and very recent[9] results, represented by the circles and squares, respectively, in Fig. 4. While the overall features at low temperatures are the same, the experimental dependences differ in the intermediate and close to T_c temperature ranges. Lack in a generally accepted microscopic model of the microwave response, we propose a description of the observed features in the entire temperature interval on the basis of a simple phenomenological model. The consequences of this model could be important both in comparing with other experiments and for constructing a microscopic theory of high-T_c superconductivity.

We thank V. F. Gantmakher and G. É. Tsydynzhapov for valuable remarks. This work was performed as part of Project 97-02-16836 of the Russian Fund for Fundamental Research and Project 96-060 of the Government program ''Superconductivity.''

[a)]e-mail: trunin@issp.ac.ru

[1]D. A. Bonn, S. Kamal, K. Zhang *et al.*, Phys. Rev. B **50**, 4051 (1994); J. Mao, D. H. Wu, J. L. Peng *et al.*, Phys. Rev. B **51**, 3316 (1995); T. Jacobs, S. Sridhar, C. T. Rieck *et al.*, J. Phys. Chem. Solids **56**, 1945 (1995).

[2] P. J. Hirschfeld and N. Goldenfeld, Phys. Rev. B **48**, 4219 (1993); H. Won and K. Maki, Phys. Rev. B **49**, 1397 (1994).
[3] S. D. Adrian, M. E. Reeves, S. A. Wolf *et al.*, Phys. Rev. B **51**, 6800 (1995); A. A. Golubov, M. R. Trunin, A. A. Zhukov *et al.*, JETP Lett. **62**, 496 (1995).
[4] C. O'Donovan and J. P. Carbotte, Phys. Rev. B **52**, 4568 (1995); H. Kim and E. J. Nicol, Phys. Rev. B **52**, 13576 (1995).
[5] P. J. Hirschfeld, W. O. Putikka, and D. J. Scalapino, Phys. Rev. B **50**, 4051 (1994).
[6] A. A. Golubov, M. R. Trunin, A. A. Zhukov *et al.*, J. Phys. I France **6**, 2275 (1996).
[7] T. Jacobs, S. Sridhar, Q. Li *et al.*, Phys. Rev. Lett. **75**, 4516 (1995); S. F. Lee, D. C. Morgan, R. J. Ormeno *et al.*, Phys. Rev. Lett. **77**, 735 (1996).
[8] M. R. Trunin, A. A. Zhukov, G. É. Tsydynzhapov *et al.*, JETP Lett. **64**, 832 (1996).
[9] H. Srikanth, B. A. Willemsen, T. Jacobs *et al.*, Report No. http://xxx. lanl. gov/abs/cond-mat/9610032.
[10] R. Cagnon, S. Pu, B. Ellman *et al.*, Phys. Rev. Lett. **78**, 1976 (1997).
[11] C. J. Stevens, D. Smith, C. Chen *et al.*, Phys. Rev. Lett. **78**, 2212 (1997).
[12] R. Liang, P. Dosanjh, D. A. Bonn *et al.*, Physica C **195**, 51 (1992).
[13] A. Erb, E. Walker, and R. Flukiger, Physica C **258**, 9 (1996).
[14] E. O. Shulz-DuBois, J. Cryst. Growth **12**, 81 (1971).
[15] M. R. Trunin, A. A. Zhukov, and A. T. Sokolov, Zh. Éksp. Teor. Fiz. **111**, 696 (1997) [JETP **84**, 383 (1997)].
[16] N. Klein, N. Tellmann, H. Schulz *et al.*, Phys. Rev. Lett. **71**, 3355 (1993).
[17] A. A. Mikhailovsky, S. V. Shulga, A. E. Karakozov *et al.*, Solid State Commun. **80**, 511 (1991); R. T. Collins, Z. Schlesinger, and F. Holtzberg, Phys. Rev. B **43**, 3701 (1991); O. V. Dolgov, E. G. Maksimov, A. E. Karakozov *et al.*, Solid State Commun. **89**, 827 (1994).

Translated by M. E. Alferieff

On the structure and stability of two-dimensional dynamic solitons in ferromagnets

A. A. Zhmudskiĭ and B. A. Ivanov
T. Shevchenko Kiev University, Kiev, Ukraine; Institute of Magnetism, Ukrainian National Academy of Sciences, 252680 Kiev, Ukraine

(Submitted 5 January 1997; resubmitted 28 May 1997)
Pis'ma Zh. Éksp. Teor. Fiz. **65**, No. 12, 899–903 (25 June 1997)

Dynamic solitons in uniaxial and orthorhombic magnets are investigated. It is shown that centrosymmetric solitons can be unstable with respect to elliptic distortions. © *1997 American Institute of Physics.* [S0021-3640(97)00912-2]

PACS numbers: 75.10.−b

1. Nonlinear excitations — topological solitons (see Ref.1) — play an important role in the physics of low-dimensional magnets.[2,3] For two-dimensional (2D) magnets with discrete degeneracy, i.e., magnets with easy-axis anisotropy ororthorhombic magnets, it is important to take account of localized stable (quite long-lived) 2D solitons.[2,3] According to experiments,[4] they determine the relaxation of magnetic disturbances and can produce peaks in the response functions.[5]

2. Let us consider an orthorhombic ferromagnet (FM) with energy of the form

$$W=\int d^2x\left\{A\left[\left(\frac{\partial\theta}{\partial x_i}\right)^2+\left(\frac{\partial\varphi}{\partial x_i}\right)^2\theta\right]+K(1+\epsilon\,\sin^2\varphi)\sin^2\,\theta\right\}, \tag{1}$$

where θ and φ determine the magnetization vector $\mathbf{m}$, $\mathbf{m}^2=1$, $m_x+im_y=\sin\theta\exp(i\varphi)$, A and K are the exchange and anisotropy constants, respectively, and ϵ describes the anisotropy in the basal plane. According to the Hobart–Derrick theorem (see Refs. 1–3), stable static 2D solitons do not exist for such a model. However, dynamic solitons (precession solitons for purely uniaxial FM with $\epsilon=0$ (Refs. 1–3) or rotation solitons[6,3]) are possible for the model (1). Their existence is due to the conservation of the z projection of the orbital angular momentum L of the magnetization field or (for $\epsilon=0$) the z projection of the total spin S. In units of Planck's constant $\hbar$ (here s is the spin of the atom, a is the lattice constant, and the square brackets denote the vector or ''cross'' product)

$$L=(s/a^2)\int d^2x(1-\cos\,\theta)[\mathbf{r},\nabla\varphi)], \quad S=(s/a^2)\int d^2x(1-\cos\,\theta). \tag{2}$$

Let us consider rotation solitons, whose existence is due to the exact (even for $\epsilon\neq0$) symmetry (1) relative to spatial rotations in the (x,y) plane of a 2D magnet. This soliton corresponds to a dynamic but stationary solution of the form $\theta(\overline{x},\overline{y})$ and $\varphi(\overline{x},\overline{y})$, where $\overline{x}=x\cos\omega t-y\sin\omega t$ and $\overline{y}=x\sin\omega t+y\cos\omega t$ are coordinates in a rotating coordinate system, to the Landau–Lifshitz equations.[6] For $\epsilon=0$ a simple cen-

trosymmetric (CS) solution can be chosen: $\theta=\theta_0(r)$ and $\varphi=\nu\chi+\varphi_0$, where ν is the topological charge, and $r=(\overline{x^2}+\overline{y^2})^{1/2}$ and $\chi=\tan^{-1}(\overline{y}/\overline{x})$ are polar coordinates in the rotating system. The function $\theta_0(r)$ can be easily found by solving an ordinary differential equation (see Refs. 1–3).

The situation is more complicated for noncentrosymmetric solutions (we shall see that they exist for both $\epsilon\neq 0$ and $\epsilon=0$). The structure of the soliton is determined by two nonlinear partial differential equations for the functions $\theta(r,\chi)$ and $\varphi(r,\chi)$. There is no general method for analyzing the localized solutions of such equations and the stability of the solutions. Soliton solutions can be constructed numerically by the molecular-dynamics method, but this requires large amounts of computer time, even with modern computers.[7] For this reason we shall analyze the structure and stability of the solitons by direct variational methods.

3. The equations for $\theta(r,\chi)$ and $\varphi(r,\chi)$ can be obtained as a condition of extremality for the auxiliary functional $\Lambda\{\theta,\varphi\}=W-\hbar\omega L$ (Ref. 6). A soliton corresponds to a conditional extremum of the energy for fixed L; $\hbar\omega$ is a Lagrange multiplier $dE(L)/dL=\hbar\omega$.

For models of FMs in which static solitons exist (see Refs. 2, 3, and 8), the functionals Λ and W are identical and the question of stability is solved simply: A minimum of the energy corresponds to a stable soliton. For a dynamic soliton the situation is more complicated: A saddle point of the functional Λ corresponds to both stable and unstable solitons (1) (see below).

In accordance with Lyapunov's direct method (see, for example, Ref. 9), a soliton is stable if there exists a Lyapunov functional $\overline{\Lambda}\{\theta,\varphi\}$ such that (i) the functional is positive-definite near the soliton solution and (ii) its time derivative, found taking account of the equations of motion, is negative or zero. Choosing the Lyapunov functional in the form of a combination of integrals of motion, $\overline{\Lambda}=\Lambda+B(L-L_0)^2$, where L_0 is the value of L in the soliton and B is a constant, the condition (ii) can be satisfied in the form $d\overline{\Lambda}/dt=0$.

The same Lyapunov functional $\overline{\Lambda}$ was chosen to analyze the stability of nontopological magnetic solitons.[9] It was found that if $\overline{\Lambda}<0$ in some region near a soliton, then the soliton is unstable. We showed that this condition of instability is also valid for centrosymmetric topological solitons (Chetaev's functional describing instability is chosen in the same form as in Ref. 9). Therefore solitons are stable if $\overline{\Lambda}>0$; otherwise, the solitons (at any rate CS solitons) are unstable.

4. We shall seek a soliton in the class of trial functions which depend on n parameters $a_1, \ldots, a_n$. Then $\Lambda\{\theta,\varphi\}\rightarrow\Lambda(a_1,\ldots,a_n,\omega)$ and the condition of an extremum takes the form of a system of n algebraic equations $\partial\Lambda/\partial a_i=0$. Once their solution $a_i^{(0)}$ has been found, the energy of the soliton $E(\omega)$ and $L(\omega)$ can be calculated and the function $E=E(L)$ can be constructed.

To analyze the stability condition (i) we investigate $\overline{\Lambda}$ for small deviations of the parameters a_i from $a_i^{(0)}$. Introducing $\alpha_i=a_i-a_i^{(0)}$, we write

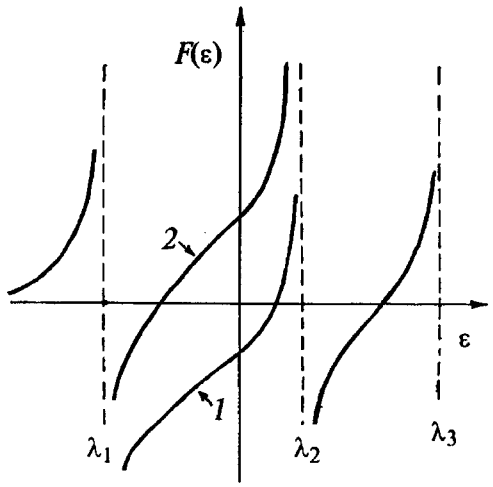

FIG. 1. The form of the function $F(\epsilon)$. The curves *1* and *2* correspond to $F(0)<0$ and $F(0)>0$.

$$\tilde{\Lambda}=\frac{1}{2}\sum_{i,k}\Lambda_{ik}\alpha_i\alpha_k+\frac{1}{2}B\left(\sum_i L_i\alpha_i\right)^2, \quad \Lambda_{ik}=\frac{\partial^2\Lambda}{\partial a_i\partial a_k}, \quad L_i=\frac{\partial L}{\partial a_i}$$

We now diagonalize the matrix Λ_{ik}, $\Lambda_{ik}=\mathrm{diag}(\lambda_1,\ldots,\lambda_n)$. The eigenvalues ϵ_i of the quadratic form $\overline{\Lambda}$ are determined by the determinant of the system $(\lambda_i-\epsilon)\alpha_i+BL_i(\Sigma_j A_j\alpha_j)=0$. Multiplying the ith equation by $L_i/B(\lambda_i-\epsilon)$, summing over i, cancelling out $\Sigma_i A_i\alpha_i$, and taking the limit $B\to\infty$, we obtain the dispersion relation $F(\epsilon)\equiv\Sigma_i L_i^2/(\lambda_i-\epsilon)=0$. Its solutions ϵ_i lie between λ_i and λ_{i+1}; see Fig. 1. Therefore if the matrix Λ_{ik} possesses two or more negative eigenvalues, then one eigenvalue $\epsilon_i<0$, and the soliton is unstable. However, if only one λ is negative, then stability is determined by the sign of $F(0)$: For $F(0)>0$ the smallest $\epsilon<0$ and for $F(0)<0$ all ϵ are positive and the soliton is stable. The quantity $F(0)$ can be related with the derivative $dL/d\omega$. Indeed, let us write $dL/d\omega=\Sigma_i L_i(da_i/d\omega)$. Differentiating the relation $\partial E/\partial a_i-\hbar\omega\partial L/\partial a_i=0$ with respect to ω, we obtain $\Sigma_k\Lambda_{ik}(da_k/d\omega)=\hbar L_i$, which implies that $dL/\hbar d\omega=F(0)$.

Therefore, just as for nontopological solitons (see Refs. 1, 2, and 9–11), the condition of stability of a topological soliton can be written in terms of the integral characteristics of the soliton. Therefore there is hope that the application of trial functions will give quite accurate results.

5. Concrete calculations were performed with a trial function of the form

$$\tan\frac{\theta}{2}=\frac{R}{r}\exp\left(-\frac{r}{b}\right)(1+C_1\cos 2\chi), \quad \varphi=\chi+\varphi_0+C_2\sin 2\chi, \tag{3}$$

which depends on five trial parameters R, b, C_1, C_2, and φ_0 and gives a good approximation of the structure of the soliton.[8] Indeed, the function $\theta_0(r)$ (3) gives a description of the Belavin–Polyakov limit, which is adequate for $R\ll\Delta$, and exponential decay of

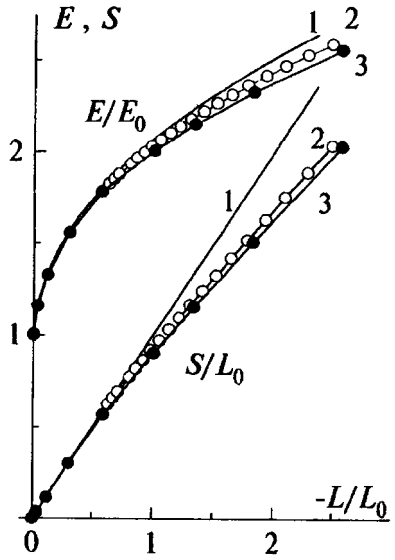

FIG. 2. The functions $E(L)$ and $S(L)$ (in units of E_0 and L_0). The curves *1* (with no symbols) and the curves *2* (○) correspond to centrosymmetric and anisotropic solitons in the limit $\epsilon \to 0$; curve *3* (●) corresponds to a soliton with $\epsilon = 0.5$.

$\theta(r)$ for $r > \Delta$, where $\Delta = \sqrt{A/K}$ is a characteristic length. The angular dependences agree with those obtained for $R \ll \Delta$ or $\epsilon \ll 1$.[8] The equations $\partial\Lambda/\partial a_i = 0$ were solved by Newton's iteration method; the initial values of the parameters a_i were set manually. The values of E, L, and S as well as the eigenvalues ofthe matrix Λ_{ik} were calculated from the quantities $a_i^{(0)}$ which were found. The functions $E(L)$ and $S(L)$ are presented in Fig. 2.

For all values of ϵ and $\omega_0 - \omega \ll \omega_0$, where ω_0 is the gap in the magnon spectrum, the soliton radius is small, $R \ll \Delta$. As $\omega \to \omega_0$, the energy of the soliton approaches $E_0 = 8\pi A$, equal to the Belavin–Polyakovenergy; here L is much smaller than the characteristic length $L_0 = 2\pi s(\Delta/a)^2$, $L_0 \gg 1$. The values of the anistropy parameters $C_1$and C_2 for $L \ll L_0$ remained small even for $\epsilon \sim 1$ ($C_1$and $C_2 < 10^{-2}$ for $\epsilon = 0.5$ and $\omega \geqslant 0.8\omega_0$, which corresponds to $L \leqslant 0.03L_0$). As the frequency decreases, the values of E and L increase, i.e., $d\omega/dL < 0$. The parameters C_1 and C_2 likewise increase for FMs with $\epsilon \neq 0$.

In the isotropic case $\epsilon = 0$, centrosymmetric solitons with C_1, $C_2 \leqslant 10^{-6}$ were easily obtained for all $\omega \leqslant \omega_0$. For CS solutions $L(\omega) = -S(\omega)$ ($L < 0$ in the soliton, see Refs. 1 and 7) and, to within 10^{-4}, the function $E(S)$ was identical to the function $E(S)$ obtained previously by integrating the equations for $\theta_0(r)$.[1–3] This demonstrates the adequacy of the method and of the trial function (3).

It was found that the solution need not be unique. (The program found one or another solution depending on the choice of the initial values of a_i.) Specifically, for small ϵ (the cases $\epsilon = 0$ and $\epsilon = 10^{-4}$ were studied, and the results were virtually identi-

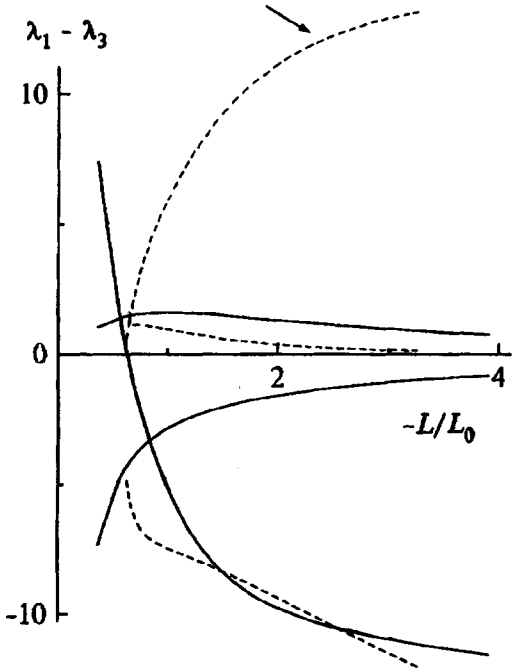

FIG. 3. The three lowest values of λ versus L for $\epsilon=0$. The solid and dashed lines correspond to centrosymmetric and anisotropic solitons. The curve marked with the arrow is plotted on a 1/2 scale.

cally) and $\omega \leqslant 0.50\omega_0$, besides centrosymmetric solutions, anisotropic solutions for which C_1 and C_2 were not small were also found. Significantly, for these solutions the value of $|L(\omega)|$ increased with decreasing ω much more rapidly than did $S(\omega)$. For this reason the functions $E(L)$ and $E(S)$ were fundamentally different: If solitons with a fixed value of S are considered, then CS solitons have a lower energy; however, if L is fixed, then the anisotropic solitons have a lower energy. For anisotropic models with values of ϵ that are not small, the value of $|L(\omega)|$ increased more rapidly than for an anisotropic soliton in a FM with $\epsilon \approx 0$. It was found that although the energy of the soliton in a FM with $\epsilon \neq 0$ and fixed ω is clearly greater than in the case $\epsilon=0$, the energy of a soliton in a FM with basal-plane anisotropy and fixed L is lower than for $\epsilon=0$.

In calculating the eigenvalues λ_i of the matrix $\Lambda_{ik}=\partial^2\Lambda/\partial a_i \partial a_k$ it was found that at least one $\lambda_i < 0$ and that solitons correspond to a saddle point of Λ. For all solitons considered, the derivative $dL/d\omega<0$, which is necessary in order for the solitons to be stable. It was found that the second condition — the fact that only one eigenvalue λ_1 is negative — is satisfied only for a soliton whose energy is minimum for fixed L. Specifically, for a CS soliton in a FM with $\epsilon \approx 0$ the second eigenvalue $\lambda_2 \geqslant 0$ only if $\omega \geqslant 0.5\omega_0$. If $\omega \leqslant 0.5\omega_0$, when an anisotropic solution appears, λ_2 changes sign and the CS soliton becomes unstable (see Fig. 3). In this case, for an anistropic soliton only λ_1 is negative, and the soliton is stable in its entire region of existence. For nontopological

multidimensional solitons, in a wide class of models the signs of λ are the same for all soliton parameters (Refs. 10, 9; see also Ref. 11).

In summary, dynamic rotation solitons with energy E close to E_0 are present in FMs with large basal-plane anisotropy. Centrosymmetric precession solitons exist in uniaxial FMs, but their symmtery is broken spontaneously for not very high energy ($E \geqslant 1.83E_0$): They become unstable and the anisotropic soliton is stable. As far as we know, the stability of topological solitons and anisotropic 2D solitons in isotropic models has not been previously discussed.

We thank Yu. S. Kivshar' for a discussion. This work was supported in part by the Ukrainian Fund for Fundamental Research under Grant No. 2.4/27.

[1] A. M. Kosevich, B. A. Ivanov, and A. S. Kovalev, Phys. Rep. **194**, 117 (1990).
[2] V. G. Bar'yakhtar and B. A. Ivanov, Soviet Scientific Rev. Sec. A – Phys. (edited by I. M. Khalatnikov) **16,** No. 3 (1992).
[3] B. A. Ivanov and A. K. Kolezhuk, Fiz. Nizk. Temp. **21,** 355 (1995) [Low Temp. Phys. **21**, 275 (1995)].
[4] F. Waldner, J. Magn. Magn. Mater. **31–34**, 1203 (1983); **54–57**, 873 (1986).
[5] B. A. Ivanov and A. K. Kolezhuk, Fiz. Nizk. Temp. **16**, 335 (1990) [Sov. J. Low Temp. Phys. **16**, 184 (1990)]; A. K. Kolezhuk and D. V. Filin, Fiz. Nizk. Temp. **20,** 1267 (1994) [Low Temp. Phys. **20**, 992 (1994)].
[6] B. A. Ivanov, JETP Lett. **56**, 118 (1992).
[7] N. Papanikolaou and W. J. Zakrzewski, Physica D **80**, 225 (1955).
[8] A. A. Zhmudskiĭ and B. A. Ivanov, Fiz. Nizk. Temp. **22,** 446 (1996) [Low Temp. Phys. **22**, 347 (1996)].
[9] B. A. Ivanov and A. L. Sukstanskii, Solid State Commun. **50**, 523 (1984).
[10] N. G. Vakhitov and A. A. Kolokolov, Izv. Vyssh. Uchebn. Zaved. Radiofiz. **16**, 1020 (1973).
[11] V. G. Makhankov, Phys. Rep. **35**, 1 (1978).

Translated by M. E. Alferieff